# Orbit Options for an Orion-Class Spacecraft Mission to a Near-Earth Object

by

**Nathan C. Shupe**

B.A., Swarthmore College, 2005

A thesis submitted to the

Faculty of the Graduate School of the

University of Colorado in partial fulfillment

of the requirements for the degree of

Master of Science

Department of Aerospace Engineering Sciences

2010

This thesis entitled:
Orbit Options for an Orion-Class Spacecraft Mission to a Near-Earth Object
written by Nathan C. Shupe
has been approved for the Department of Aerospace Engineering Sciences

_____
Daniel Scheeres

_____
Prof. George Born

_____
Assoc. Prof. Hanspeter Schaub

Date _____

The final copy of this thesis has been examined by the signatories, and we find that both the
content and the form meet acceptable presentation standards of scholarly work in the above
mentioned discipline.

Shupe, Nathan C. (M.S., Aerospace Engineering Sciences)

Orbit Options for an Orion-Class Spacecraft Mission to a Near-Earth Object

Thesis directed by Prof. Daniel Scheeres

Based on the recommendations of the Augustine Commission, President Obama has proposed a vision for U.S. human spaceflight in the post-Shuttle era which includes a manned mission to a Near-Earth Object (NEO). A 2006-2007 study commissioned by the Constellation Program Advanced Projects Office found that a number of suitable mission targets already exist in the database of known NEOs, and many of these objects can be reached for less $\Delta v$ than would be required for a mission to the lunar surface.

The objective of this thesis is to pick up where the previous Constellation study left off by considering what orbit options are available for an Orion-class spacecraft upon arrival at a NEO. A model including multiple perturbations (solar radiation pressure, solar gravity, non-spherical mass distribution of the central body) to two-body dynamics is constructed to numerically integrate the motion of a satellite in close proximity to a small body in an elliptical orbit about the Sun. Analytical limits derived elsewhere in the literature for the thresholds on the size of the orbit required to maintain stability in the presence of these perturbing forces are verified by the numerical model. Simulations about NEOs possessing various physical parameters (size, shape, rotation period, etc...) are then used to empirically develop general guidelines for establishing orbits of an Orion-class spacecraft about a NEO. It is found that an Orion-class spacecraft can orbit NEOs at any distance greater than the NEO surface height and less than the maximum semi-major axis allowed by the solar radiation pressure perturbation, provided that the ellipticity perturbation is sufficiently weak (met if the NEO is relatively round and/or has a long rotation period) for orbits falling below the minimum threshold for guarding against its effects. NEOs as small as $\approx 20$ m in diameter can be orbited by an Orion-class spacecraft, provided their rotation period is not too long ($< 30$ hours) if the ellipticity perturbation is strong. There are cases of small, very slowly

rotating NEOs that cannot be orbited by an Orion-class spacecraft at any distance, but generally these NEOs are required to have severely elongated shapes in order to maintain the strength of the ellipticity perturbation in spite of the longer rotation period. Finally, terminator frozen orbits are found to be the best orbit option for a manned mission to a NEO, since their stability in the face of multiple perturbations provides an ideal platform for conducting scientific observations of the NEO and launching astronaut excursions to the NEO surface.

## Dedication

To my wife, Sabrina, whose daily support and warm encouragement have sustained me throughout this process. The passion you have for your own work and the excellence you consistently achieve in its practice were my guiding lights in this endeavor. You not only made this thesis possible, but you also made it better.

To my Mom and Dad, who instilled in me a desire to set lofty goals in life and gave me the confidence I needed to realize them. The stars seem to be getting closer all of the time.

And to my sister, Ellen, whose own unfailing work ethic continues to inspire me to learn more and better myself. I hope I have done you proud with this work.

## Acknowledgements

I am enormously in debt to Dr. Scheeres, who served as the chair of my committee and was my primary advisor on this thesis. His patient and thoughtful guidance were invaluable in helping me to focus the objective of this research, and his seemingly limitless supply of useful tips and suggestions not only improved the quality of the thesis, but also helped to ensure that it was completed on time.

I would also like to thank Dr. Born, who as my academic advisor was there to help direct this research at its inception. I especially appreciate his willingness to allow me unfettered freedom in selection of my topic, even when my final selection fell outside of his research area.

And lastly, I would like to express my gratitude to Dr. Schaub for serving on my thesis committee and for providing a number of insightful comments during my defense. His suggestions improved the quality of my thesis and have given me some exciting ideas for future work on this research topic.

# Contents

**Chapter**

# Tables

**Table**

# Figures

**Figure**

# Chapter 1

# Introduction

## 1.1    Motivation for NEO exploration

> Early in the next decade, a set of crewed flights will test and prove the systems required for exploration beyond low Earth orbit. And by 2025, we expect new spacecraft designed for long journeys to allow us to begin the first-ever crewed missions beyond the Moon into deep space. So we'll start – we'll start by sending astronauts to an asteroid for the first time in history. By the mid-2030s, I believe we can send humans to orbit Mars and return them safely to Earth. And a landing on Mars will follow. And I expect to be around to see it.

In this excerpt from a speech given on April 15, 2010 at the John F. Kennedy Space Center, President Barack Obama outlined several of the milestones from his vision for the future of U.S. human spaceflight. Among the objectives identified by the President was the goal to complete by the end of the next decade the first-ever manned mission outside of cis-lunar space. The target of such a mission will be a nearby asteroid, selected from the population of small-body objects in close proximity to the Earth known as Near-Earth Objects (NEOs).

The impetus for the inclusion of a manned NEO mission in the President's spaceflight vision came from the final report issued by the Review of U.S. Human Spaceflight Plans Committee [4]. This body – made up of various experts from industry and academia and chaired by former Lockheed Martin chairman and CEO Norman Augustine (after whom the commission is often named) – was commissioned by the Executive Office of the President to assist in the definition and articulation of a plan for U.S. human spaceflight in the post-Shuttle era. Among its findings, the Augustine Commission reported that Mars is the best candidate for the ultimate destination of human space-

flight, and that return missions to the Moon would likely be required in order to verify the systems and procedures for landing, ascent and surface operations. However, recognizing that missions to Mars will be much longer in duration and distance than missions to the Moon, the Augustine Commission also recommended that several other intermediate missions be included in what they called the Flexible Path to Mars (see Figure 1.1). This plan provides an incremental buildup to a
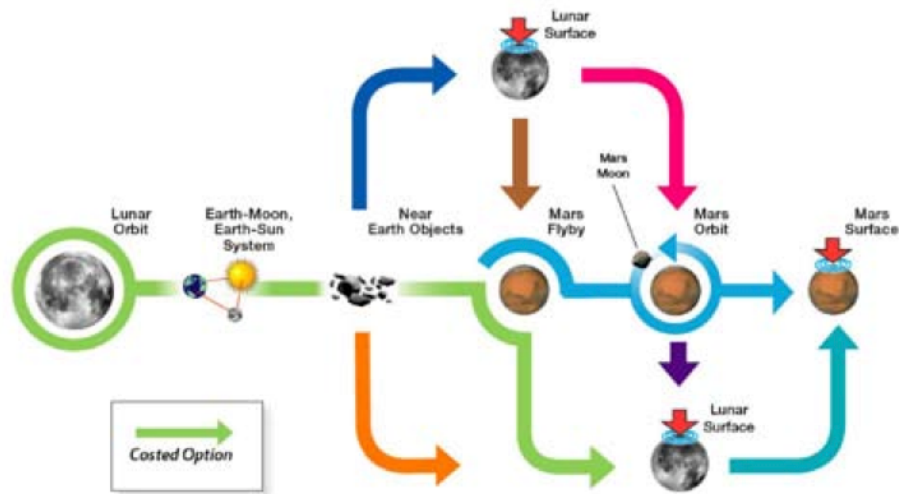


Figure 1.1: Options for the Flexible Path strategy proposed by the Augustine Commission. [Image sourced from the Review of U.S. Human Spaceflight Plans Committee]

full-up manned mission to Mars by scheduling several intermediate missions of increasing duration, the targets for which lie outside of lunar orbit. These missions provide the opportunity to carefully and thoroughly investigate the impacts of deep-space travel, including the long-term effects of radiation exposure and a zero-gravity environment on astronauts. The destinations suggested by the commission for these missions were purposely selected based on the magnitude of their expected science return, as well as their likely utility in future space operations. In particular, NEOs were included for many reasons, some of which are listed below:

- Because asteroids are believed to be the remnants of a planetary body which failed to form

in the region between the orbits of Mars and Jupiter, the materials which make them up are believed to be representative of the composition of the early Solar System.

- Based on absorption features observed in the spectra measured from C-type asteroids, it is believed that this class of asteroids may possess water. If this hypothesis is confirmed by in-situ measurements of the asteroid surface, then asteroids could become a valuable extra-terrestrial resource for the raw materials necessary for space travel.

- Given that the orbits of many NEOs intersect Earth's orbit, there is a non-zero probability that one of them will one day impact the Earth. In order to refine our plan for defending Earth against such a catastrophic event, it will be important to understand the interior characteristics of asteroids.

- The microgravity environment of a NEO provides a low cost and risk testbed for new space technologies. The shallow gravity well of NEOs makes them among the most energetically accessible bodies in the inner solar system, and also allows them to be more forgiving when errors in the design of approach trajectories and maneuvers for close proximity operations inevitably occur.

.

### 1.1.1    Unmanned missions

Even before the Augustine Commission issued its final report with a recommendation to conduct missions to NEOs, the benefits of visiting these small bodies was already well understood and accepted within the community, as evidenced by the plethora of past and current unmanned missions sent to asteroids and comets. A list of all past and current unmanned missions to asteroids and comets is provided in Table 1.1. Notice that past missions merely conducted a fly-by of the target small body, with the exception of the NEAR mission to 433 Eros and the Hayabusa mission to 25143 Itokawa. The NEAR spacecraft initialized into a elliptical orbit about 433 Eros, which was deemed an acceptable mission design given the significant size of the asteroid ($\approx 10$ km in

diameter, an order of magnitude larger than most NEOs). However, because 25413 Itokawa is significantly smaller than 433 Eros, the design selected for the Hayabusa mission called for frequent thruster firings to be used to hold the spacecraft in a fixed position relative to the NEO-Sun fixed frame [21]. Both the spacecraft and the controllers (due to the communications delay between the controllers and the spacecraft) encountered difficulties while trying to maintain this configuration during close proximity operations at the asteroid [5].

### 1.1.2    Manned missions

In nearly every phase of the U.S. human spaceflight program, ranging from orbital rendezvous with the Gemini spacecraft to Hubble Space Telescope servicing missions with the Space Shuttle, NASA astronauts have demonstrated strong acumen in precision maneuvering during close proximity operations. Therefore, it would seem reasonable to expect that a human crew piloting a spacecraft in proximity to an asteroid would be able to successfully mitigate many of the challenges experienced by the Hayabusa mission at 25413 Itokawa. Human crews would also be able to more readily collect samples from the asteroid. The Hayabusa spacecraft was designed to return two small samples from 25413 Itokawa, and initial analysis of the returned sampler container has shown that the spacecraft successfully captured and returned approximately 1500 microscopic (10 microns in diameter) grains of surface material from Itokawa [6]. In a manned mission, astronauts could venture outside of the spacecraft and conduct Extra-vehicular Activites (EVAs) on the surface, collecting many macroscopic (centimeters in diameter) samples from a diverse set of surface locations. Astronauts would also be able to readily test out different tools/strategies for obtaining samples from the NEO, which would increase the likelihood of successful sample return on the current mission and enhance the scientific returns from future missions. For these reasons, it is expected that a manned mission to a NEO would provide a much more significant science return than an equivalent unmanned mission.

## 1.2    Characterization of NEOs

### 1.2.1    Population characterization

The NEO population is made up of all solar system asteroids and comets in heliocentric orbits having a perihelion of less than 1.3 AU. Since this population is dominated by asteroids, and also because comets are unsuitable targets for manned exploration due to their volatile nature, for the purposes of this study the population of NEOs is considered limited to all Near Earth Asteroid (NEA) objects.

Only a small subset of all NEOs are accessible for a manned mission given current or future proposed launch capabilities. These objects are all members of a subset of the NEO group known as Potentially Hazardous Asteroids (PHAs), which are defined as NEAs that are projected to pass within 0.05 AU of the Earth and have a absolute magnitude (apparent visual magnitude that would be measured by an observer at a distance of 1 AU from the object) $H \leq 22.0$. For an assumed value for the surface albedo of an asteroid, this brightness criterion establishes a size threshold for asteroids to be members of this group.

The NASA Jet Propulsion Laboratory (JPL) maintains a database of information characterizing small body objects, made up of all known asteroids and comets. The database can be queried through an online interface available at `http://ssd.jpl.nasa.gov/sbdb_query.cgi#x`. Orbit elements and physical parameter data for all known PHAs were extracted from this database, which as of November 11, 2010 consisted of 1167 objects.

In order to select a reference orbit to be used for all NEOs in this study, a plot was generated for the two dimensional distribution of the values for the semi-major axis and eccentricity of all known PHA orbits. This plot is shown in Figure 1.2 for $a < 4$ AU and $e < 1$ (note that two PHAs have $a > 4$ AU and are excluded from this plot). Since PHAs accessible for a manned mission must be in orbits fairly similar to that of the Earth, the distribution for consideration was further limited to only those asteroids whose orbits have a semi-major axis of $a < 1.2$ AU and $e < 0.3$. A plot of this restricted distribution is shown in Figure 1.3. There appears to be a group of objects

clustered around $a = 1.05$ AU and $e = 0.15$, so these values are selected for the NEO reference orbit in this study.

Distribution of PHA Orbit Elements
1165 Objects Selected
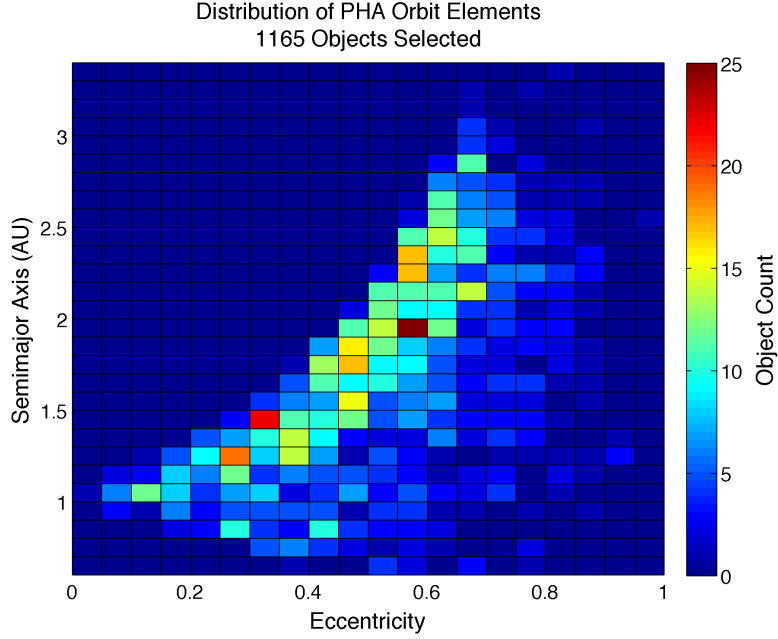


Figure 1.2: Distribution of orbital elements for all PHAs.

## 1.2.2    Physical properties

Just like other celestial bodies, NEOs can possess a wide range of physical properties. In the context of modeling a NEO, some of the most important parameters are its size and shape, rotation period and axis direction, and mass density (assumed to be uniform throughout the body). The cumulative distributions of the rotation period and sphere equivalent diameter parameters are computed for PHA objects in the JPL small body database having defined values for these parameters. Unfortunately, the limitations of our current observational tools do not allow for estimation of these parameters for most NEOs, so these distributions represent only a small subset of the entire population of NEOs and PHAs. Figure 1.4 shows that approximately half of the PHA population has a sphere-equivalent diameter less than 1 km, and approximately 95% has a diameter less than 5 km. Figure 1.5 shows that approximately half of the PHA population has a rotation
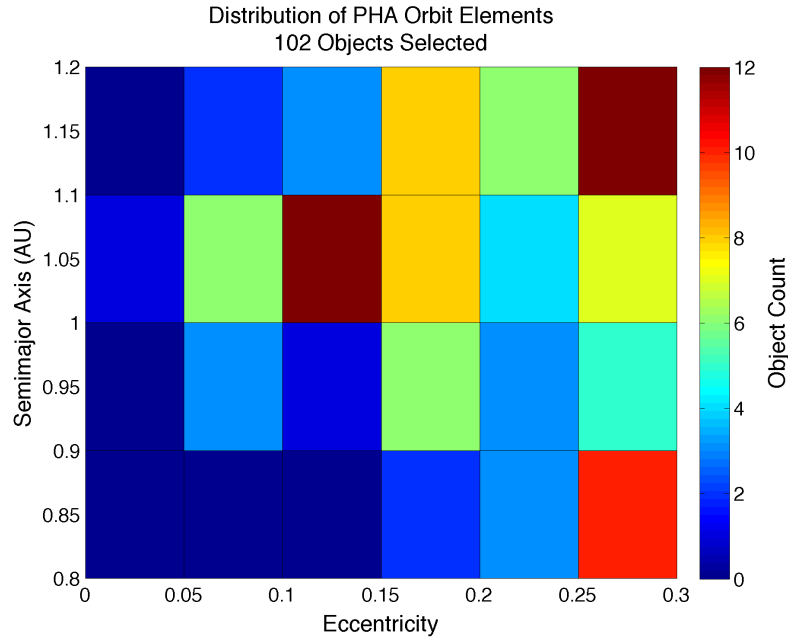
Figure 1.3: Distribution of PHA orbital elements for $a < 1.2$ AU and $e < 0.3$.
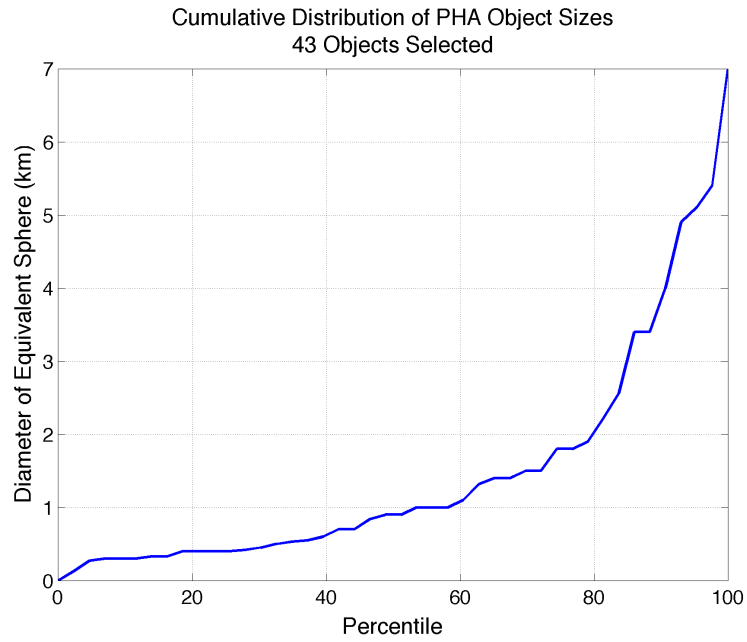


Figure 1.4: Distribution of PHA sphere equivalent diameters.
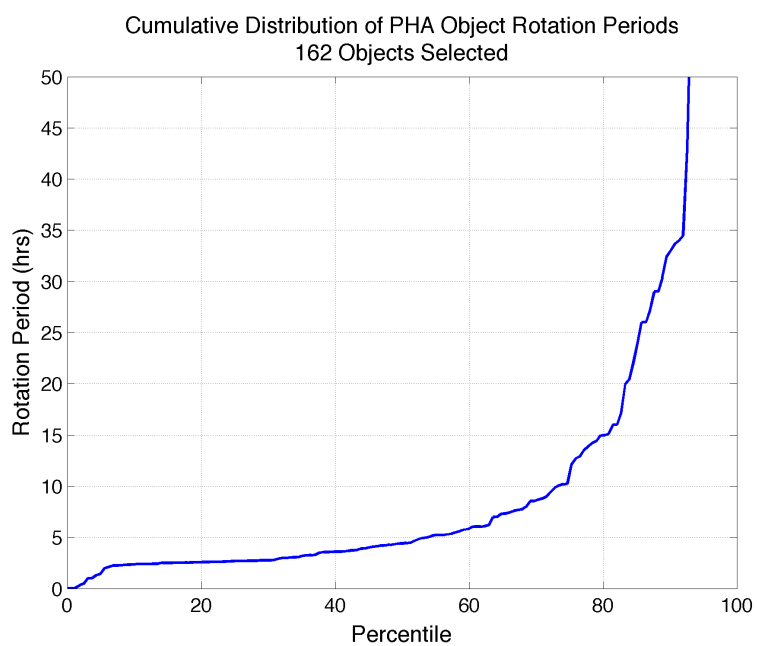
Figure 1.5: Distribution of PHA rotation periods.

period less than 5 hours, and approximately 90% has a period less than 35 hours.

The NASA Planetary Data System maintains a collection of asteroid data sets, available for download at `http://sbn.psi.edu/pds/archive/asteroids.html`. A histogram is computed for all known asteroid mass densities available in the data set `EAR_A_5_DDR_ASTEROID_DENSITIES_V1_1` and is shown in Figure 1.6. The figure clearly shows that most asteroids have a density $\rho \leq 2.5$
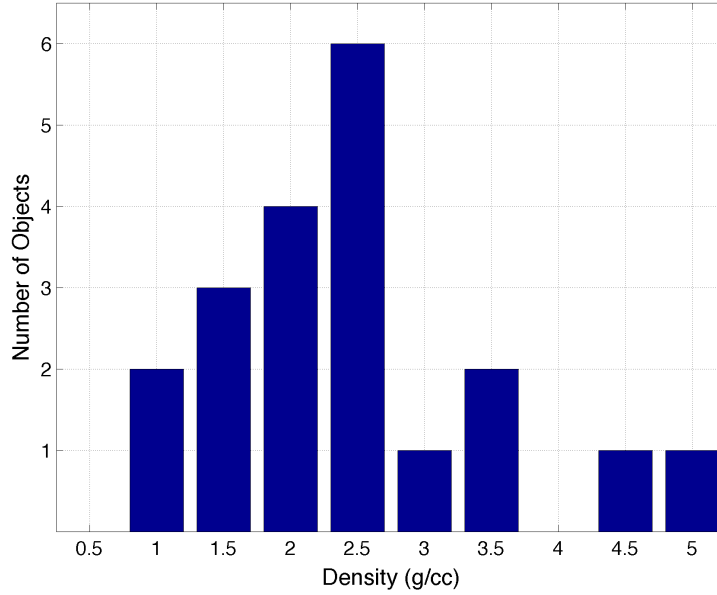


Figure 1.6: Distribution of asteroid mass densities.

g/cc, so a value of 2.0 g/cc is selected for all NEOs modeled in this study.

## 1.3    Previous Work

Prior to the effective cancellation of the Constellation Program in the 2010 NASA Authorization Act (S. 3729), a study was commissioned by the Advanced Project Office in 2006-2007 to examine the feasibility of sending the Orion CEV to a NEO [17]. This study focused on the identification of potential NEO targets for several launch scenarios using the latest Ares launch systems and Orion spacecraft designs of that time. The study concluded that a number of suitable NEO candidates for a manned mission have already been discovered, and that the number of candidates

will continue to increase as more NEOs are discovered in future surveys of the asteroid population.

The objective of this thesis to pick up where the previous NASA study left off by investigating the available trajectory options for an Orion-class S/V in close proximity to a NEO. In particular, the availability and sustainability of Orion orbits at NEOs possessing various physical parameters will be investigated.

Table 1.1: Past and Current Unmanned Missions to Asteroids and Comets[†]

| Target Body | Event | | Mission Details | | |
| --- | --- | --- | --- | --- | --- |
| | Type | Date | Name | Launch | Status |
| 1 Ceres | arrival | 2015-Feb | Dawn | 2007-Sep-27 | cruise |
| 67P/Churyumov-Gerasimenko | landing | 2014-Nov | Rosetta | 2004-Mar-02 | cruise |
| 67P/Churyumov-Gerasimenko | rendezvous | 2014-Aug | Rosetta | 2004-Mar-02 | cruise |
| 4 Vesta | departure | 2012-Jul | Dawn | 2007-Sep-27 | cruise |
| 4 Vesta | arrival | 2011-Jul | Dawn | 2007-Sep-27 | cruise |
| 9P/Tempel 1 | fly-by | 2011-Feb-14 | Stardust-NExT | 1999-Feb-06 | cruise |
| 103P/Hartley 2 | fly-by | 2010-Nov-04 | EPOXI | 2005-Jan-12 | cruise |
| 21 Lutetia | fly-by | 2010-Jul-10 | Rosetta | 2004-Mar-02 | cruise |
| 25143 Itokawa (1998 SF36) | sample-return | 2010-Jun-13 | Hayabusa (MUSES-C) | 2003-May-09 | cruise |
| 2867 Steins (1969 VC) | fly-by | 2008-Sep-05 | Rosetta | 2004-Mar-02 | cruise |
| 25143 Itokawa (1998 SF36) | departure | 2007-Apr-25 | Hayabusa (MUSES-C) | 2003-May-09 | cruise |
| 81P/Wild 2 | sample-return | 2006-Jan-15 | Stardust | 1999-Feb-06 | complete |
| 25143 Itokawa (1998 SF36) | arrival | 2005-Sep-12 | Hayabusa (MUSES-C) | 2003-May-09 | cruise |
| 9P/Tempel 1 | impact/fly-by | 2005-Jul-04 | Deep Impact | 2005-Jan-12 | complete |
| 81P/Wild 2 | fly-by | 2004-Jan-02 | Stardust | 1999-Feb-06 | complete |
| 5535 Annefrank (1942 EM) | fly-by | 2002-Nov-02 | Stardust | 1999-Feb-06 | complete |
| 19P/Borrelly | fly-by | 2001-Sep-22 | Deep Space 1 | 1998-Oct-24 | complete |
| 433 Eros (1898 DQ) | rendezvous | 2000-Feb-14 | NEAR | 1996-Feb-17 | complete |
| 9969 Braille (1992 KD) | fly-by | 1999-Jun-28 | Deep Space 1 | 1998-Oct-24 | complete |
| 253 Mathilde | fly-by | 1997-Jun-27 | NEAR | 1996-Feb-17 | complete |
| 243 Ida | fly-by | 1993-Aug-28 | Galileo | 1989-Oct-18 | complete |
| 951 Gaspra (1916 S45) | fly-by | 1991-Oct-29 | Galileo | 1989-Oct-18 | complete |
| 1P/Halley | fly-by | 1986-Mar-14 | Giotto | 1985-Jul-02 | complete |
| 1P/Halley | fly-by | 1986-Mar-11 | Sakigake | 1985-Jan-07 | complete |
| 1P/Halley | fly-by | 1986-Mar-09 | Vega 2 | 1984-Dec-21 | complete |
| 1P/Halley | fly-by | 1986-Mar-08 | Suisei | 1985-Aug-18 | complete |
| 1P/Halley | fly-by | 1986-Mar-06 | Vega 1 | 1984-Dec-15 | complete |
| 21P/Giacobini-Zinner | fly-by | 1985-Sep-11 | ISEE 3/ICE | 1978-Aug-12 | complete |

[†]Data taken from `http://ssd.jpl.nasa.gov/?targets` on November 24, 2010.

<center>## Chapter 2</center>

<center>## Model</center>

## 2.1 NEO orbit model

The unperturbed Keplerian orbit of the NEO about the Sun is given by the trajectory equation

$$d = \frac{P}{1 + E \cos \nu},$$ (2.1)

where $d$ is the distance measured from the Sun to the NEO, $P$ and $E$ are the semi-latus rectum and eccentricity parameters of the NEO Keplerian orbit respectively, and $\nu$ is the true anomaly angle measured from the periapsis direction to the position vector of the NEO in the Sun-centered inertial frame. The angular velocity, or time rate of change of the true anomaly angle, of the NEO is related to its angular momentum $h$ by

$$\dot{\nu} = \frac{h}{d^2}.$$ (2.2)

By substituting $h = \sqrt{\mu_\odot P}$, where $\mu_\odot \approx 1.327 \times 10^{11}$ km$^3$/s$^2$ is the gravitational parameter for the Sun, Eq. 2.2 can be rewritten as

$$\dot{\nu} = \frac{\sqrt{\mu_\odot P}}{d^2}.$$ (2.3)

The angular velocity vector is given by $\mathbf{\Omega} = \dot{\nu}\hat{\mathbf{z}}$ where $\hat{\mathbf{z}}$ is a unit vector normal to the orbit plane and aligned with the angular momentum vector, $\mathbf{h} = \mathbf{d} \times \dot{\mathbf{d}}$. The $\hat{\mathbf{x}}$ unit vector points in the

perihelion direction, and the final unit vector, $\hat{\mathbf{y}} = \hat{\mathbf{z}} \times \hat{\mathbf{x}}$, completes the orthogonal basis set for the Sun-centered inertial reference frame $\mathcal{N} = \{\mathcal{O}, \hat{\mathbf{x}}, \hat{\mathbf{y}}, \hat{\mathbf{z}}\}$, where $\mathcal{O}$ is the frame origin. Two other reference frames are defined, both anchored to the NEO center of mass position as the NEO orbits the Sun. The first of these NEO-centered frames is defined to be fixed inertially relative to the NEO and is denoted as $\mathcal{N}' = \{\mathcal{O}', \hat{\mathbf{x}}, \hat{\mathbf{y}}, \hat{\mathbf{z}}\}$. Though this frame is non-rotating, it is not truly inertial, since the frame origin $\mathcal{O}'$ is accelerated according to the motion of the NEO about the Sun. The second NEO-centered frame is defined to rotate with the NEO position vector, and is denoted as $\mathcal{B} = \{\mathcal{O}', \hat{\mathbf{d}}, \hat{\mathbf{z}} \times \hat{\mathbf{d}}, \hat{\mathbf{z}}\}$ where $\hat{\mathbf{d}}$ is a unit vector directed along the Sun-NEO position vector $\mathbf{d}$. A schematic of the Sun-NEO-satellite system is depicted in Figure 2.1.

Later, when expressing the satellite equations of motion in a frame rotating with the NEO motion about the Sun, the time derivative of the angular velocity vector, $\dot{\boldsymbol{\Omega}}$, will be required. The magnitude of this vector can be computed by differentiating with respect to time the expression for the true anomaly rate given in Equation 2.3:

$$\ddot{\nu} = -2\sqrt{\mu_\odot P}\frac{\dot{d}}{d^3}. \tag{2.4}$$

Differentiating with respect to time the trajectory equation in Equation 2.1 yields:

$$\dot{d} = \frac{d\dot{\nu}E\sin\nu}{1 + E\cos\nu}. \tag{2.5}$$

And then substituting for $\dot{d}$ in Equation 2.4 from Equation 2.5 and simplifying using Equation 2.1 gives:

$$\ddot{\nu} = -2\sqrt{\frac{\mu_\odot}{P}}\frac{E\dot{\nu}\sin\nu}{d}. \tag{2.6}$$

Since the direction of the angular momentum vector does not vary, the time derivative of the angular momentum vector must be parallel with the angular momentum vector. Therefore, the time derivative of the angular momentum vector is written as $\dot{\boldsymbol{\Omega}} = \ddot{\nu}\hat{\mathbf{z}}$.
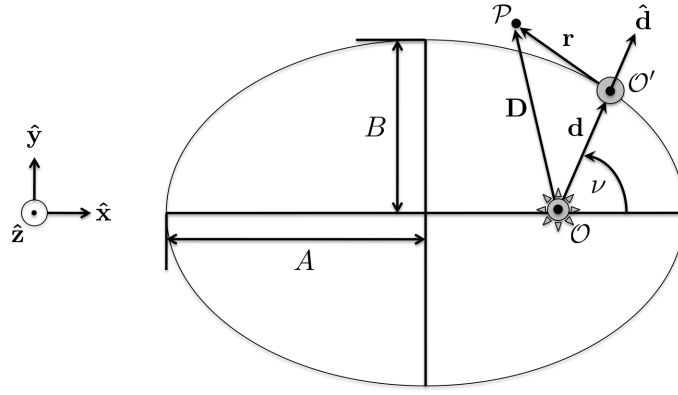
Figure 2.1: Notional schematic of the Sun-NEO-satellite system. The Sun is located at point $\mathcal{O}$, the NEO at point $\mathcal{O}'$, and the satellite at point $\mathcal{P}$. The Sun-centered inertial frame is denoted as $\mathcal{N} = \{\mathcal{O}, \hat{\mathbf{x}}, \hat{\mathbf{y}}, \hat{\mathbf{z}}\}$, the NEO-centered non-rotating frame as $\mathcal{N}' = \{\mathcal{O}', \hat{\mathbf{x}}, \hat{\mathbf{y}}, \hat{\mathbf{z}}\}$, and the NEO-centered rotating frame as $\mathcal{B} = \{\mathcal{O}', \hat{\mathbf{d}}, \hat{\mathbf{z}} \times \hat{\mathbf{d}}, \hat{\mathbf{z}}\}$. Note that semi-latus rectum and eccentricity parameters in Equation 2.1 are related to the semi-major axis $A$ and semi-minor axis $B$ of the ellipse by $P = B^2/A$ and $E = \sqrt{1 - (B/A)^2}$.

## 2.2    NEO gravity model

### 2.2.1    Two body

Under the assumption of a spherically symmetric mass distribution, the NEO can be modeled as a point mass, and the inertial two-body acceleration applied to the satellite is given by

$$\mathbf{a}_{2\text{body}} = -\frac{G(m + M)}{|\mathbf{r}|^3}\mathbf{r} \approx -\frac{\mu_{\text{N}}}{|\mathbf{r}|^3}\mathbf{r}, \tag{2.7}$$

where $G = 6.67428 \times 10^{-11}$ m$^3$ kg$^{-1}$ s$^{-2}$ is the gravitational constant, $\mu_{\text{N}} = GM$ is the gravitational parameter for a NEO of mass $M$, and $\mathbf{r} = \mathbf{D} - \mathbf{d}$ is the position vector of the satellite measured relative to the NEO position. Note that in order to substitute $\mu_{\text{N}}$ for $G(m + M)$, it is assumed that $M \gg m$. Depending on the size of the NEO, this may or may not be a good assumption.

### 2.2.2    Non-spherical mass distribution

Precise mass estimates are not available for nearly all known NEOs (Eros and Itokawa are the only exceptions in the JPL small body database), but given their small size it is fair to assume that their masses are many orders of magnitude smaller than other celestial bodies in our solar system (e.g., planets or moons). Because their masses are so small, the gravitational fields of NEOs are far too weak to overcome rigid body forces in order to achieve a spherical shape consistent with a hydrostatic equilibrium state (pressure forces exactly balancing gravitational forces). Consequently, the true shapes of NEOs are likely to depart significantly from spheres. To model the perturbing acceleration associated with a non-spherical distribution of the NEO mass, a simple tri-axial ellipsoid model is assumed for the NEO shape. A NEO-centered fixed (rotating) reference frame is defined to be aligned with the principal body axes and is denoted $\mathcal{R} = \{\mathcal{O}', \hat{\mathbf{s}}, \hat{\mathbf{q}}, \hat{\mathbf{p}}\}$. The NEO shape and NEO-centered fixed frame $\mathcal{R}$ are depicted in Figure 2.2.

The elements of the body inertia matrix can be computed using the following equation from [25]:
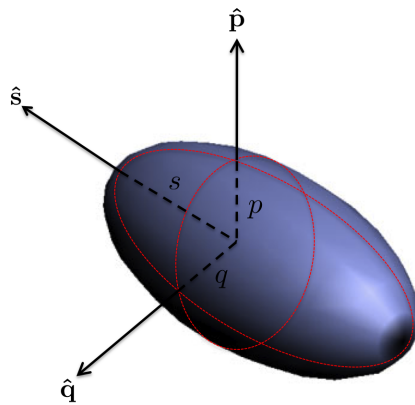
Figure 2.2: Schematic of an ellipsoidal model for the NEO. The NEO-centered fixed reference frame (rotates with the NEO) is denoted $\mathcal{R} = \{\mathcal{O}', \hat{\mathbf{s}}, \hat{\mathbf{q}}, \hat{\mathbf{p}}\}$. Because the basis vectors of this reference frame are aligned with the principal body axes, the body inertia matrix expressed in this frame is diagonalized, with $I_{33} \geq I_{22} \geq I_{11}$. [Image adapted from the Wikimedia Commons file: `http://commons.wikimedia.org/wiki/File:Ellipsoid_3d.jpg`]

$$I_{ij} = \int_V \rho(\mathbf{r}) \left( \delta_{ij} \sum_k x_k^2 - x_i x_j \right) \mathrm{d}V \tag{2.8}$$

where

$$\delta_{ij} = \begin{cases} 0, & i \neq j \\ 1, & i = j \end{cases} \tag{2.9}$$

is the Kronecker delta. Because the $\mathcal{R}$ frame is aligned with the principal body axes, the integral in Equation 2.8 evaluates to zero for all off-diagonal elements ($i \neq j$). Assuming the mass density function is constant throughout the mass distribution, $\rho(\mathbf{r}) = \rho$ and the diagonal elements of the inertia matrix are then found to be:

$$
\begin{aligned}
I_{11} &= \rho \int_V (y^2 + z^2)\,\mathrm{d}x\,\mathrm{d}y\,\mathrm{d}z &&= \frac{1}{5}M(q^2 + p^2), \\
I_{22} &= \rho \int_V (x^2 + z^2)\,\mathrm{d}x\,\mathrm{d}y\,\mathrm{d}z &&= \frac{1}{5}M(p^2 + s^2), \\
I_{33} &= \rho \int_V (x^2 + y^2)\,\mathrm{d}x\,\mathrm{d}y\,\mathrm{d}z &&= \frac{1}{5}M(s^2 + q^2),
\end{aligned}
\tag{2.10}
$$

where $M = \rho V = \rho \frac{4}{3}\pi abc$ is the total mass and $\{s, q, p\}$ are the semi-principal axes of the ellipsoid. From [21], the second order and degree gravity coefficients for the ellipsoid are related to its inertia moments by:

$$
\begin{aligned}
C_{20} &= -\frac{1}{2}(2I_z - I_x - I_y), \tag{2.11} \\
C_{22} &= \frac{1}{4}(I_y - I_x), \tag{2.12}
\end{aligned}
$$

where $[I_x, I_y, I_z] = \frac{1}{M}[I_{11}, I_{22}, I_{33}]$ are the mass-normalized moments of inertia. Note that the other gravity coefficents – $C_{10}, C_{11}, S_{11}, C_{21}, S_{21}, S_{22}$ – all evaluate to zero because the NEO reference frame has been defined to be anchored at the NEO center of mass and oriented along the principal axes of inertia of the NEO body ([26], [11]). Also from [21], the potential due to the 2nd order and

degree gravitational field perturbation is given for the general case of the ellipsoid polar axis offset

from the polar axis $\hat{\mathbf{z}}$ of the reference coordinate frame:

$$R = -\frac{\mu_N}{2r^3}C_{20}\left[1 - 3(\hat{\mathbf{r}} \cdot \hat{\mathbf{p}})^2\right] + \frac{3\mu_N}{r^3}C_{22}\left[(\hat{\mathbf{r}} \cdot \hat{\mathbf{s}})^2 - (\hat{\mathbf{r}} \cdot \hat{\mathbf{q}})^2\right]. \tag{2.13}$$

The acceleration due to the perturbation potential is found by taking the partial derivative of the

potential with respect to the position vector:

$$\mathbf{a}_{\mathrm{mdist}} = \frac{\partial R}{\partial \mathbf{r}} = \begin{bmatrix} \frac{\partial R}{\partial x} & \frac{\partial R}{\partial y} & \frac{\partial R}{\partial z} \end{bmatrix}^T. \tag{2.14}$$

By substituting $\mathbf{r}/r = \hat{\mathbf{r}}$ and analytically evaluating the partial derivative, the acceleration vector

due to the potential in Equation 2.13 is found to be:

$$
\begin{aligned}
\mathbf{a}_{\mathrm{mdist}} = \ & \frac{3\mu_N}{2r^5}C_{20}\left\{\left[1 - \frac{5}{r^2}(\mathbf{r} \cdot \hat{\mathbf{p}})^2\right]\mathbf{r} + 2(\mathbf{r} \cdot \hat{\mathbf{p}})\hat{\mathbf{p}}\right\} \\
& -\frac{3\mu_N}{r^5}C_{22}\left\{\frac{5}{r^2}\left[(\mathbf{r} \cdot \hat{\mathbf{s}})^2 - (\mathbf{r} \cdot \hat{\mathbf{q}})^2\right]\mathbf{r} - 2\left[(\mathbf{r} \cdot \hat{\mathbf{s}})\hat{\mathbf{s}} - (\mathbf{r} \cdot \hat{\mathbf{q}})\hat{\mathbf{q}}\right]\right\}
\end{aligned}
\tag{2.15}
$$

The ellipsoid polar axis $\hat{\mathbf{p}}$, defined as the axis about which the body inertia is greatest, is

expressed in $\mathcal{N}'$ frame components as:

$$\hat{\mathbf{p}} = \sin\beta\sin\alpha\hat{\mathbf{x}} - \sin\beta\cos\alpha\hat{\mathbf{y}} + \cos\beta\hat{\mathbf{z}}, \tag{2.16}$$

where $\beta = \cos^{-1}(\hat{\mathbf{p}} \cdot \hat{\mathbf{z}})$ measures the obliquity and $\alpha = \cos^{-1}\left(\frac{(\hat{\mathbf{z}}\times\hat{\mathbf{p}})\cdot\hat{\mathbf{x}}}{|\hat{\mathbf{z}}\times\hat{\mathbf{p}}|}\right)$ the right ascension of the

$\hat{\mathbf{p}}$ direction (see Figure 2.3 for a depiction of these reference angles). The polar axis is assumed

to be inertially fixed, constantly oriented in the direction specified by Equation 2.16. The NEO

is assumed to rotate uniformly and exclusively about its polar axis, at a rate of $\omega = \frac{2\pi}{P}$ (rad/sec)

where $P$ (sec) is the period of the NEO rotation. This rotation, as well as the rotations associated

with the obliquity and right ascension angles, can be represented by the following direction cosine

matrices for single-axis rotations:
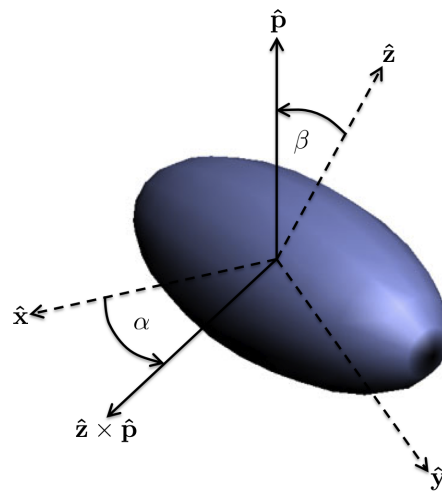
Figure 2.3: Orientation of the NEO polar axis relative to the $\mathcal{N}'$ frame. [Image adapted from the Wikimedia Commons file: `http://commons.wikimedia.org/wiki/File:Ellipsoid_3d.jpg`]

$$[M_1(\theta)] = \begin{bmatrix} 1 & 0 & 0 \\ 0 & \cos\theta & \sin\theta \\ 0 & -\sin\theta & \cos\theta \end{bmatrix}, \tag{2.17}$$

$$[M_3(\theta)] = \begin{bmatrix} \cos\theta & \sin\theta & 0 \\ -\sin\theta & \cos\theta & 0 \\ 0 & 0 & 1 \end{bmatrix}, \tag{2.18}$$

where $\theta$ is the angle swept out by the rotation. The combined rotation which transforms the $\mathcal{N}'$ frame to the $\mathcal{R}$ frame is a (3-1-3) Euler rotation, given by:

$$[RN'] = [M_3(\omega t)][M_1(\beta)][M_3(\alpha)], \tag{2.19}$$

where $\omega t$ (rad) is the angle swept out by the NEO rotation over a period of $t$ seconds. At an arbitrary time $t$ since the reference epoch, this rotation matrix can be used to transform individual vectors from the $\mathcal{N}'$ frame to the $\mathcal{R}$ frame, or alternatively it can be used to express the $\mathcal{R}$ frame basis vectors as a linear combination of the $\mathcal{N}'$ basis vectors:

$$\begin{bmatrix} \hat{\mathbf{s}} \\ \hat{\mathbf{q}} \\ \hat{\mathbf{p}} \end{bmatrix} = [RN'] \begin{bmatrix} \hat{\mathbf{x}} \\ \hat{\mathbf{y}} \\ \hat{\mathbf{z}} \end{bmatrix}. \tag{2.20}$$

## 2.3    Third body gravity model

The third body perturbing the motion of the NEO-orbiting satellite is the Sun. The form of this perturbing acceleration is given in [26]:

$$\mathbf{a}_{3\text{body}} = \mu_\odot \left( \frac{\mathbf{d}}{|\mathbf{d}|^3} - \frac{\mathbf{d}+\mathbf{r}}{|\mathbf{d}+\mathbf{r}|^3} \right), \tag{2.21}$$

where $\mathbf{d}+\mathbf{r} = \mathbf{D}$ is the position vector of the satellite and $\mathbf{d}$ the position vector of the NEO, both measured relative to the Sun's position. This first term in Equation 2.21 is the acceleration of the

NEO and the second term is the acceleration of the satellite, both due to the Sun's gravity.

## 2.4    Solar radiation pressure model

The momentum of a body having rest mass $m_0$ and momentum $p$ is related to its total energy $E$ by Einstein's relativistic energy-momentum equation

$$E = \sqrt{(pc)^2 + (m_0 c^2)^2},$$
(2.22)

where $c \approx 2.99792 \times 10^8$ m/s is the speed of light constant. For a photon, $m_0 = 0$, so the momentum of a photon is given by $p = E/c$. By Newton's second law, a force can be expressed as the time rate of change of momentum, so the force $F$ imparted by a photon, or more specifically a collective group of photons in the form of electromagnetic radiation, is given by

$$F = \frac{\mathrm{d}}{\mathrm{dt}}\left(\frac{E}{c}\right) = \frac{1}{c}\frac{\mathrm{d}E}{\mathrm{dt}} = \frac{P}{c},$$
(2.23)

where $P$ is power in units of Watts (W). Pressure is defined as the force per unit area applied in a direction perpendicular to a reference surface, so the radiation pressure equation is given by

$$p_{\mathrm{SR}} = \frac{P/c}{A_\perp} = \frac{f}{c},$$
(2.24)

where $f$ is the the radiative power per unit area (W/m$^2$), also known as radiative flux, incident on a surface oriented perpendicular to the incoming radiation. As light emitted by the Sun propagates through space, its power is diluted geometrically by an inverse square law,

$$f = \frac{L_\odot}{4\pi|\mathbf{D}|^2},$$
(2.25)

where $L_\odot = 3.839 \times 10^{26}$ W is the time-averaged luminosity (or power) of the Sun. From [26], the acceleration due to the solar radiation pressure, $a_{\mathrm{SRP}}$, from radiation incident on a body of mass $m$ (kg) is given by

$$\mathbf{a}_{\text{SRP}} = \frac{p_{\text{SR}} c_{\text{R}} A_{\perp \odot}}{m} \frac{\mathbf{D}}{|\mathbf{D}|}, \tag{2.26}$$

where $A_{\perp \odot}$ (m$^2$) is the cross-sectional area perpendicular to the direction of the solar radiation and $c_{\text{R}}$ is the reflectivity,

$$c_{\text{R}} = \begin{cases} 0, & \text{transparent} \\ 1, & \text{blackbody} \\ 2, & \text{mirror} \end{cases} \tag{2.27}$$

By substituting Eqs. 2.24 and 2.25 into Eq. 2.26 and defining $B = m/A_{\perp \odot}$ (kg/m$^2$) to be the mass to area ratio of the body, the acceleration due to solar radiation pressure can be expressed as

$$\mathbf{a}_{\text{SRP}} = \frac{L_{\odot}}{4\pi c} \frac{c_{\text{R}}}{B} \frac{\mathbf{d} + \mathbf{r}}{|\mathbf{d} + \mathbf{r}|^3}, \tag{2.28}$$

for the NEO-centered $\mathcal{N}'$ frame, where $\mathbf{d} + \mathbf{r} = \mathbf{D}$. Note that this model for the solar radiation pressure force approximates the perturbed body as a flat plate with its surface normal oriented perpendicular to the direction of the incident photon flux.

## 2.5 Equations of motion

### 2.5.1 Non-rotating reference frame

The acceleration of the satellite as measured in the non-rotating reference frame $\mathcal{N}'$ is found by summing the contributions from two-body gravity, non-spherical mass distribution, solar gravity, and solar radiation pressure.

$$\begin{aligned} \ddot{\mathbf{r}} &= \mathbf{a}_{2\text{body}} + \mathbf{a}_{3\text{body}} + \mathbf{a}_{\text{SRP}} + \mathbf{a}_{\text{mdist}} \\ &= \left[ -\mu_{\text{N}} \frac{\mathbf{r}}{|\mathbf{r}|^3} + \left( \frac{L_{\odot}}{4\pi c} \frac{c_{\text{R}}}{B} - \mu_{\odot} \right) \frac{\mathbf{d} + \mathbf{r}}{|\mathbf{d} + \mathbf{r}|^3} + \frac{\partial R}{\partial \mathbf{r}} \right] - \left[ -\mu_{\odot} \frac{\mathbf{d}}{|\mathbf{d}|^3} \right] \\ &= [\ddot{\mathbf{D}}] - [\ddot{\mathbf{d}}] \end{aligned} \tag{2.29}$$

Therefore, the acceleration of the satellite as measured in the $\mathcal{N}'$ frame is found to be the difference of the inertial acceleration of the satellite location, point $\mathcal{P}$, and the $\mathcal{N}'$ frame origin, point $\mathcal{O}'$, both

measured in the inertial $\mathcal{N}$ frame centered at the Sun. In the limit as $m \to M$, the acceleration of the NEO due to the gravity field of the satellite gravity cannot be ignored, and the equations of motion for the NEO become:

$$\ddot{\mathbf{d}} = -\mu_\odot \frac{\mathbf{d}}{|\mathbf{d}|^3} + \mu_{\text{sat}} \frac{\mathbf{r}}{|\mathbf{r}|^3}. \tag{2.30}$$

Note that Equation 2.30 is only applicable for extremely small NEOs.

### 2.5.2    Rotating reference frame

For certain analytical applications, it is useful to express the equations of motion in the $\mathcal{B}$ reference frame which rotates with the NEO position vector. From [19], the Transport Theorem used to transform the derivative of a generic vector $\mathbf{x}$ from a reference frame $\mathcal{B}$ to another reference frame $\mathcal{N}$ related to the other by a relative angular velocity vector $\omega_{\mathcal{B}/\mathcal{N}}$ is given as:

$$\frac{^{\mathcal{N}}\text{d}}{\text{dt}}(\mathbf{x}) = \frac{^{\mathcal{B}}\text{d}}{\text{dt}}(\mathbf{x}) + \omega_{\mathcal{B}/\mathcal{N}} \times \mathbf{x}, \tag{2.31}$$

where $\frac{^{\mathcal{N}}\text{d}}{\text{dt}}$ is the derivative taken in the $\mathcal{N}$ frame, and $\frac{^{\mathcal{B}}\text{d}}{\text{dt}}$ is the derivative taken in the $\mathcal{B}$ frame. For our application, the satellite velocity measured in the $\mathcal{B}$ frame is related to the velocity measured in the $\mathcal{N}'$ frame by:

$$\begin{aligned}
\dot{\mathbf{r}} &= \frac{^{\mathcal{N}'}\text{d}}{\text{dt}}(\mathbf{r}) \\
&= \frac{^{\mathcal{B}}\text{d}}{\text{dt}}(\mathbf{r}) + \omega_{\mathcal{B}/\mathcal{N}'} \times \mathbf{r} \\
&= (\dot{\mathbf{r}})_{\mathcal{B}} + \mathbf{\Omega} \times \mathbf{r}
\end{aligned} \tag{2.32}$$

Similarly, the satellite acceleration measured in the $\mathcal{B}$ frame is related to the acceleration measured in the $\mathcal{N}'$ frame by:

$$\begin{aligned}
\ddot{\mathbf{r}} &= \frac{^{\mathcal{N}'}\text{d}}{\text{dt}}(\dot{\mathbf{r}}) \\
&= \frac{^{\mathcal{B}}\text{d}}{\text{dt}}(\dot{\mathbf{r}}) + \omega_{\mathcal{B}/\mathcal{N}'} \times \dot{\mathbf{r}} \\
&= (\ddot{\mathbf{r}})_{\mathcal{B}} + 2\mathbf{\Omega} \times (\dot{\mathbf{r}})_{\mathcal{B}} + \mathbf{\Omega} \times \mathbf{\Omega} \times \mathbf{r} + \dot{\mathbf{\Omega}} \times \mathbf{r}
\end{aligned} \tag{2.33}$$

Although it is possible to integrate the equations of motion in the rotating reference frame, it is often preferable to integrate them in the non-rotating frame because the initial conditions in the non-rotating reference frame can be expressed as orbital elements. Once the motion has been integrated in the non-rotating frame, a transformation can be applied to express the position and velocity in the rotating reference frame. The rotation matrix for transforming from the $\mathcal{N}'$ basis to the $\mathcal{B}$ basis is the direction cosine matrix for a single-axis rotation of true anomaly angle $\nu$ about the $\hat{\mathbf{z}}$ axis:

$$[BN'] = [M_3(\nu)]. \tag{2.34}$$

Using the rotation matrix from Equation 2.34 and the Transport Theorem from Equation 2.31, the position and velocity vectors can be transformed from the $\mathcal{N}'$ to the $\mathcal{B}$ frame as follows:

$$
\begin{aligned}
(\mathbf{r})_\mathcal{B} &= [BN']\mathbf{r}, \\
(\dot{\mathbf{r}})_\mathcal{B} &= [BN'] \left( \dot{\mathbf{r}} - \boldsymbol{\Omega} \times \mathbf{r} \right).
\end{aligned}
\tag{2.35}
$$

## 2.6 Model parameters

The software implementation of the model described in the previous sections allows for nearly every parameter to be specified as a run-time input (with the exception of the orbit elements describing the orientation of the NEO orbit relative to the inertial $\mathcal{N}$ frame, since that frame is defined to be aligned with the NEO heliocentric orbit). However, due to the limitations of time and computation speed, some parameters had to remain fixed in order to constrain the parameter space and complete the studies for this thesis. Those parameters that were selected to remain constant are summarized in Table 2.1, and those that remained free to be adjusted are listed in Table 2.2. Future research in this area of study could investigate how the behavior of the candidate orbits identified in Chapter 3 would be affected by changes to one or more of the fixed parameters.

## 2.7 Numerical integration schema

The system state vector is made up by the state vectors of the satellite and the NEO. The satellite state vector is given by its position and velocity as measured in the $\mathcal{N}'$ frame, and the NEO state vector by its position and velocity as measured in the $\mathcal{N}$ frame. Because the unperturbed NEO orbit is fully described by the analytic solution to the two-body problem given in Equation 2.1, the NEO state is included in the system state vector and integrated numerically merely for convenience. The system state vector $\mathbf{X}$ and the time-differentiated system vector $\dot{\mathbf{X}}$ are written as:

$$\mathbf{X} = \begin{bmatrix} \mathbf{r} \\ \dot{\mathbf{r}} \\ \mathbf{d} \\ \dot{\mathbf{d}} \end{bmatrix}, \qquad \dot{\mathbf{X}} = \begin{bmatrix} \dot{\mathbf{r}} \\ \ddot{\mathbf{r}} \\ \dot{\mathbf{d}} \\ \ddot{\mathbf{d}} \end{bmatrix}, \tag{2.36}$$

where the values of $\ddot{\mathbf{r}}$ and $\ddot{\mathbf{d}}$ are computed from Equation 2.29. At each time step in the simulation, $t_n$, the initial conditions of the system are specified by $\mathbf{X}_n$ and are used to solve for the time-differentiated state $\dot{\mathbf{X}}_n$. Then using the MATLAB® [18] ordinary differential equation solver **ode45**, which implements an adaptive step Runge-Kutta 4(5) method, the system state is integrated forward to the next time step, $t_{n+1}$. Before proceeding with the next integration, the new system state, $\mathbf{X}_{n+1}$, is verified against the requirements that the satellite does not impact the NEO surface or escape NEO orbit. The procedures used for verifying these requirements are listed below:

- Requirement #1: Satellite does not impact the NEO surface.

    (1) Rotate the satellite position vector into the $\mathcal{R}$ frame:
    $$^{\mathcal{R}}\mathbf{r}_{n+1} = [RN'(t_{n+1})]\mathbf{r}_{n+1},$$
    $$= r_1\hat{\mathbf{s}} + r_2\hat{\mathbf{q}} + r_3\hat{\mathbf{p}}.$$

    (2) Check that the satellite position falls outside the NEO surface:
    $$\frac{r_1^2}{s^2} + \frac{r_2^2}{q^2} + \frac{r_3^2}{p^2} > 1.$$

- Requirement #2: Satellite does not escape from NEO orbit.

  (1) Check that the satellite position does not exceed the smaller of the Hill radius and 5x the initial orbit semi-major axis:

$$|\mathbf{r}_{n+1}| \leq \begin{cases} 5a_0, & 5a_0 < r_{\text{Hill}} \\ r_{\text{Hill}}, & r_{\text{Hill}} < 5a_0 \end{cases}$$

If both requirements are met, then $\mathbf{X}_{n+1} \to \mathbf{X}_n$ and the integration procedure is repeated for the next time step. Typically, the satellite and NEO motion are propagated for one full revolution of the NEO orbit ($T_{\text{N}} = 2\pi\sqrt{A^3/\mu_\odot}$) in order to sample all possible system geometries.

## 2.8    Initial conditions

Since the satellite motion about the NEO is integrated in a non-rotating frame, the initial conditions for the satellite orbit can be expressed as orbital elements instead of Cartesian position and velocity vectors. Expressing the initial state in orbital elements facilitates the design of useful orbits, as it is often much easier to track and make adjustments to orbits expressed in orbital elements. In particular, a class of orbits that remain frozen relative to the rotating $\mathcal{B}$ frame can be quickly designed using orbit elements for the initial conditions.

In [20] and [21], two families of orbits were found that maintain a fixed or *frozen* orientation relative to the Sun-NEO line. These orbits would be desirable for a manned mission to a NEO because they are stable in the presence of a strong solar radiation pressure perturbation. The safety of the spacecraft and the astronauts is put at risk if perpetual thruster firings are required to maintain the orbit about the NEO, so an orbit which is designed to be naturally stable in this environment provides a significant mitigation of this risk.

The first family of frozen orbits are referred to as **Terminator Frozen Orbits**, and are so named because the satellite orbits in a plane perpendicular to the Sun-NEO line known as the terminator plane. For these orbits, if the angular momentum vector $\hat{\mathbf{h}}$ points toward the Sun, then periapsis points in the $+\hat{\mathbf{z}}$ direction. If, however, the angular momentum vector $\hat{\mathbf{h}}$ points away from

the Sun, then periapsis points in the $-\hat{\mathbf{z}}$ direction.

The second family of orbits are called **Ecliptic Frozen Orbits** because the satellite orbits the NEO in the ecliptic plane, which is the plane of the NEO's orbit about the Sun. For these orbits, periapsis can point either toward or away from the Sun, along the Sun-NEO line described by $\hat{\mathbf{d}}$.

The algorithms used for computing the initial conditions for orbits in either of these frozen orbit families are provided below.

- Terminator Frozen Orbit

  (1) Select a semi-major axis (m): $a$

  (2) Solve for the eccentricity:
  $$\Lambda = \frac{3L_\odot}{8B\pi c}\sqrt{\frac{a}{P\mu_{\mathrm{N}}\mu_\odot}},$$
  $$\psi = \tan^{-1}\Lambda,$$

  $$e = \cos\psi.$$

  (3) Set the inclination (deg) for a polar orbit: $i = 90°$

  (4) Set the RAAN (deg) to place the satellite orbit plane perpendicular to the Sun-NEO line:
  $$\hat{\mathbf{n}} = \begin{cases} \dfrac{\hat{\mathbf{d}} \times \hat{\mathbf{z}}}{|\hat{\mathbf{d}} \times \hat{\mathbf{z}}|}, & \hat{\mathbf{h}} \text{ pointing toward the Sun} \\ \dfrac{\hat{\mathbf{z}} \times \hat{\mathbf{d}}}{|\hat{\mathbf{z}} \times \hat{\mathbf{d}}|}, & \hat{\mathbf{h}} \text{ pointing away from the Sun} \end{cases},$$
  $$\mathrm{RAAN} = \begin{cases} \cos^{-1}(\hat{\mathbf{n}} \cdot \hat{\mathbf{x}}), & \hat{\mathbf{n}}(2) \geq 0 \\ 360° - \cos^{-1}(\hat{\mathbf{n}} \cdot \hat{\mathbf{x}}), & \hat{\mathbf{n}}(2) < 0 \end{cases}.$$

  (5) Set the $\omega_p$ (deg) as follows:
  $$\omega_p = \begin{cases} 90°, & \hat{\mathbf{h}} \text{ pointing toward the Sun} \\ -90°, & \hat{\mathbf{h}} \text{ pointing away from the Sun} \end{cases}.$$

  (6) Select a true anomaly angle (deg): $\nu$

- Ecliptic Frozen Orbit

  (1) Select a semi-major axis (m): $a$

  (2) Solve for the eccentricity:

  $$\Lambda = \frac{3L_\odot}{8B\pi c}\sqrt{\frac{a}{P\mu_N\mu_\odot}},$$

  $$\psi = \tan^{-1}\Lambda,$$

  $$e = \sin\psi.$$

  (3) Set the inclination (deg) for an equatorial orbit:

  $$i = \begin{cases} 0°, & \hat{\mathbf{e}} \text{ pointing toward the Sun} \\ 180°, & \hat{\mathbf{e}} \text{ pointing away from the Sun} \end{cases}.$$

  (4) Set the RAAN (deg) (somewhat arbitrarily, since the RAAN is undefined for an equatorial orbit): $\text{RAAN} = 0°$

  (5) Set the $\omega_p$ (deg) to place periapsis along the NEO-Sun line:

  $$\hat{\mathbf{e}} = \begin{cases} -\hat{\mathbf{d}}, & \hat{\mathbf{e}} \text{ pointing toward the Sun} \\ \hat{\mathbf{d}}, & \hat{\mathbf{e}} \text{ pointing away from the Sun} \end{cases},$$

  * $\hat{\mathbf{e}}$ pointing toward the Sun:

  $$\omega_p = \begin{cases} \cos^{-1}(\hat{\mathbf{x}}\cdot\hat{\mathbf{e}}), & \hat{\mathbf{e}}(2) \geq 0 \\ 360° - \cos^{-1}(\hat{\mathbf{x}}\cdot\hat{\mathbf{e}}), & \hat{\mathbf{e}}(2) < 0 \end{cases}.$$

  * $\hat{\mathbf{e}}$ pointing away from the Sun:

  $$\omega_p = \begin{cases} \cos^{-1}(\hat{\mathbf{x}}\cdot\hat{\mathbf{e}}), & \hat{\mathbf{e}}(2) \leq 0 \\ 360° - \cos^{-1}(\hat{\mathbf{x}}\cdot\hat{\mathbf{e}}), & \hat{\mathbf{e}}(2) > 0 \end{cases}.$$

  (6) Select a true anomaly angle (deg): $\nu$

Table 2.1: Model Fixed Parameters

| Object | Parameter | Value | Notes |
|---|---|---|---|
| NEO | $\rho$ (g/cc) | 2.0 | Justification given in Chapter 1 |
| | $\alpha$ (deg) | 45 | Arbitrary if propagating for a full NEO orbit; should allow the satellite to sample every azimuth angle |
| | $\beta$ (deg) | 45 | Representative; should be varied in future work |
| | $A$ (AU) | 1.05 | Justification given in Chapter 1 |
| | $E$ | 0.15 | Ditto |
| | $I$ (deg) | 0 | $\mathcal{N}$ frame $\hat{\mathbf{z}}$ is aligned with NEO orbit $\hat{\mathbf{h}}$ |
| | RAAN (deg) | 0 | RAAN is undefined for an equatorial orbit |
| | $\omega_p$ (deg) | 0 | $\omega_p$ is undefined for an equatorial orbit |
| | $\nu$ (deg) | 270 | Arbitrary if propagating for a full NEO orbit |
| Orion-Class Spacecraft | $M$ (kg) | 20000 | CEV Capsule [15] + Service Module (dry mass + propellant) [2] |
| | $A_{\perp\odot}$ (m$^2$) | 50 | Capsule cross-section + Solar Array area [15] |
| | $c_{\mathrm{R}}$ | 1 | Blackbody |
| Astronaut | $M$ (kg) | 220 | 175 lb Body + Shuttle class space suit [1] |
| | $A_{\perp\odot}$ (m$^2$) | 0.9 | 1.8 m height x 0.5 m width |
| | $c_{\mathrm{R}}$ | 1 | Blackbody |

Table 2.2: Model Free Parameters

| Object | Parameter | Description |
|---|---|---|
| NEO | $[s, p, q]$ (m) | Ellipsoid semi-principal axes |
| | $P$ (hr) | Rotation period |
| Satellite | $a$ (m) | Semi-major axis |
| | $e$ | Eccentricity |
| | $i$ (deg) | Inclination |
| | RAAN (deg) | Right ascension of ascending node |
| | $\omega_p$ (deg) | Argument of periapsis |
| | $\nu$ (deg) | True anomaly angle |

# Chapter 3

# Analysis

## 3.1    Stability definition

Before proceeding with analyses of the orbit studies conducted with the numerical model described in the previous chapter, it is necessary to define what stability means for satellite orbits about a small body within the context of this thesis. A rigorous definition of stability such as that which would be used for a control problem (e.g. Lagrange, Lyapunov, etc...) is not applied to these cases. Instead, a stable small body orbit is defined rather generally as a satellite trajectory for which the osculating elements of its orbit can be used to provide a reasonably accurate estimate of the position (and velocity) of the satellite position at a later time. Consequently, it is possible to have an orbit bound to the small body (motion is dominated by gravitational attraction of the small body) which is unstable, provided its osculating orbital elements are varying rapidly throughout its motion. The goal of this research is to find orbits which are both bound to the small body and stable in the presence of multiple perturbing forces.

## 3.2    Limiting radii

### 3.2.1    Sphere of influence

The Sphere of Influence (SOI), often used in the patched conic method for generating satellite trajectories in a multi-body gravitational environment, approximates the size of the region around a body within which the motion of a satellite can be fully described by two-body dynamics. Given

a body of mass $m_1$ and another body of mass $m_2$, and assuming that $m_2 \ll m_1$, the radius of the SOI for $m_2$ is calculated by equating the ratio of the two-body accelerations for the satellite about $m_1$ and $m_2$ to the ratio of the disturbing accelerations due to $m_2$ and $m_1$. The equation for the SOI radius is given in [7] as:

$$r_{\mathrm{SOI}} = d \left( \frac{m_2}{m_1} \right)^{2/5},$$ (3.1)

where $d$ is the distance between $m_1$ and $m_2$. It should be noted that a satellite at a position outside of this SOI can still potentially orbit the secondary body, but its motion at that position cannot be solely described by two-body dynamics. However, if the satellite does lie within the sphere, the perturbation on its motion due to the gravitational attraction of a third body can be effectively ignored.

### 3.2.1.1 Parametric study

For the Sun-NEO system, $m_2$ is the mass of the NEO, $m_1 = M_\odot = 1.9891 \times 10^{30}$ kg is the mass of the Sun, and $d$ is the distance from the Sun to the NEO. For various Sun-NEO distances and NEO diameters, contours of equal $r_{\mathrm{SOI}}/R_{\mathrm{N}}$ are plotted in Fig. 3.1, where $R_{\mathrm{N}}$ is the sphere-equivalent radius of the NEO. This radius can be derived from the total volume of the NEO $V_{\mathrm{N}}$ using:

$$R_{\mathrm{N}} = \left( \frac{3}{4\pi} V_{\mathrm{N}} \right)^{1/3}.$$

In the plot, a ratio value of $\leq 1$ indicates that the third body perturbation due to the Sun should be included for all possible orbits about the NEO. Notice that for all of the Sun-NEO distances and NEO diameters evaluated for the plot, there are ranges of orbit radii over which the third body acceleration can be excluded from the satellite equations of motion.
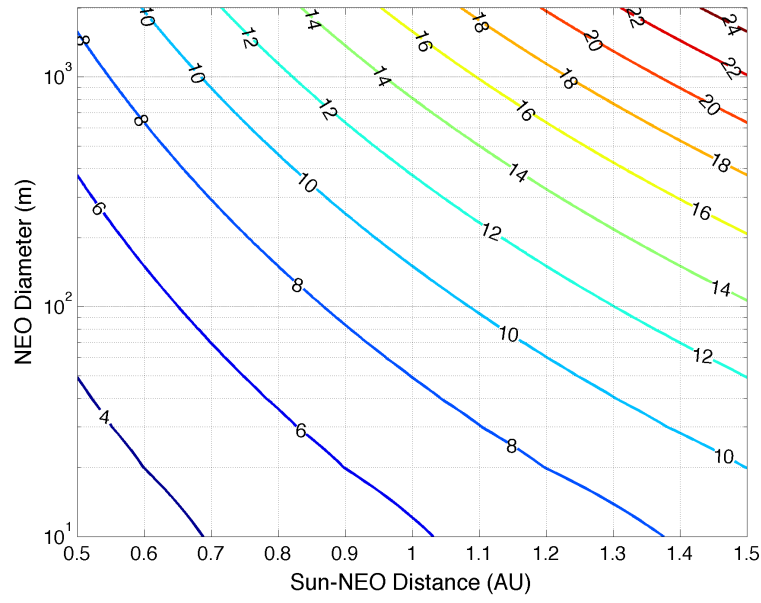
Figure 3.1: Contour plot of $r_{\mathrm{SOI}}/R_{\mathrm{N}}$ as computed by Eq. 3.1. Note that the NEO is assumed to have a constant mass density of $\rho = 2.0$ g/cc.

### 3.2.1.2    Numerical verification

To verify that the third body perturbation can be effectively ignored within the SOI radius, a test was conducted using the NEO+satellite orbit model described in Chapter 2 with the perturbations due to solar radiation pressure and a non-spherical NEO mass distribution deactivated. The NEO is assumed to be on the reference orbit specified in Table 2.1 except for a slightly higher eccentricity (0.2). Its size is specified by a sphere-equivalent radius of 300 m, and its mass density is assumed to be constant and equal to $\rho = 2.0$ g/cc. Plugging the mass of the NEO,

$$M = \rho \frac{4}{3} \pi R_{\mathrm{N}}^3,$$

and the periapsis distance of its orbit into Equation 3.1, the SOI radius is found to be $r_{\mathrm{SOI}} = 3323$ m. The satellite is initialized in a circular ecliptic orbit about the NEO of size $a = 2500$ m in order to place it well within the NEO SOI.

For this test, two cases were executed. The first and second case both propagated the spacecraft state using two-body dynamics, but the second case also included the third body perturbation of the Sun. The differences between the results (shown in Figure 3.2 below) are extremely small, which confirms that the effect of the third body perturbation on the motion of a satellite within the SOI is negligible.

### 3.2.2    Hill sphere

The Hill Sphere approximates the region surrounding a body in which the body's gravitational attraction is the dominant attractive force acting on a nearby satellite. Unlike the region bounded by the SOI, the Hill sphere region does not preclude significant influence from a disturbing third body, provided that the gravitational attraction of the third body does not exceed that of the satellite's central body. Because the Hill sphere permits this third body influence, it is larger than the SOI, but the motion of a satellite within this expanded region is no longer solely governed by two body dynamics. The boundary of the region is defined to be distance at which the direct gravity of the central body is balanced by the tidal forces of the third body in a reference frame
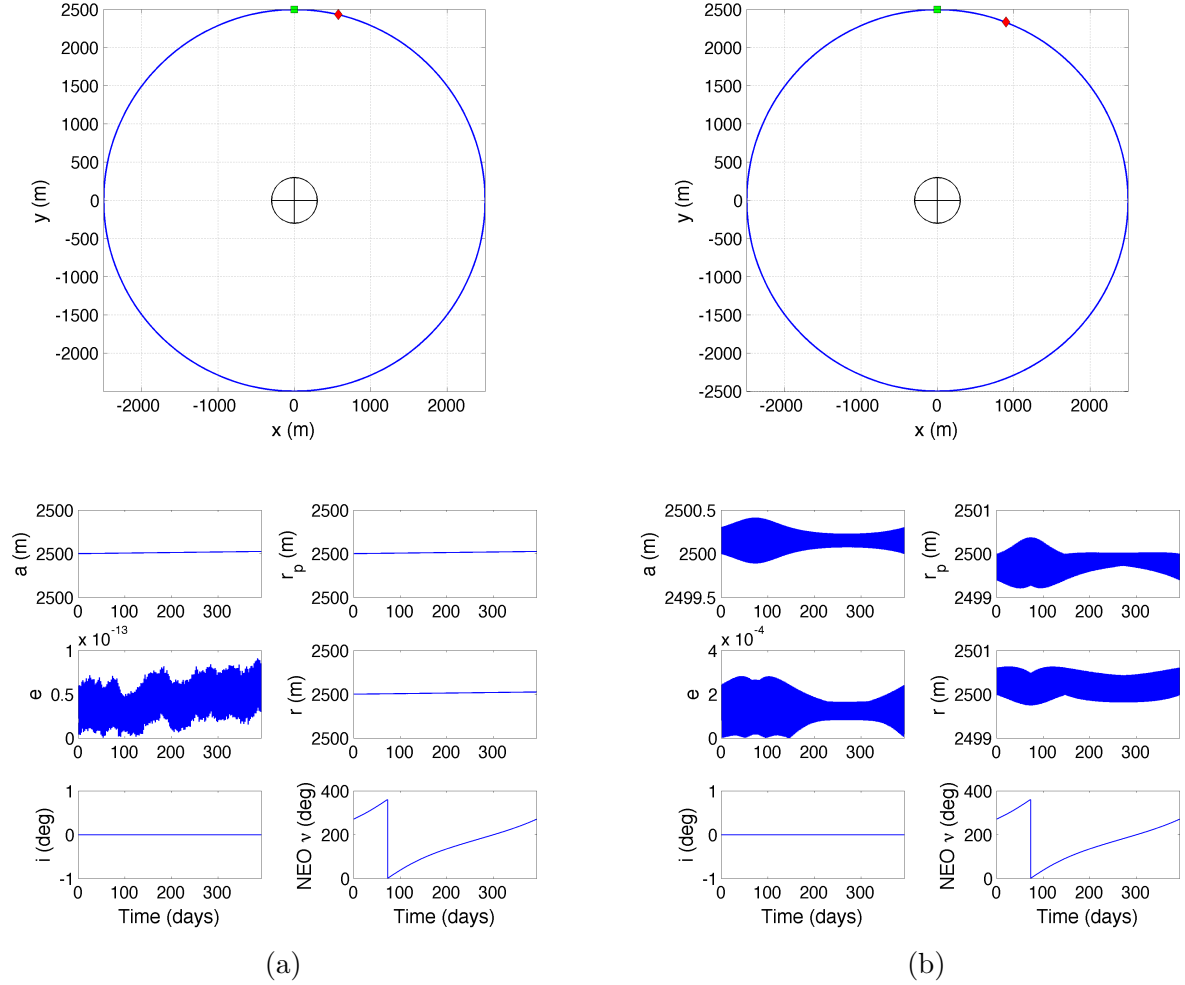
Figure 3.2: Results from the SOI test cases: (a) satellite motion propagated without any perturbations; (b) satellite motion propagated with a solar gravity perturbation. For each test case, the integrated satellite trajectory as viewed in the $\mathcal{B}$ frame is shown (the Sun lies at a fixed position on the negative x-axis in this reference frame), as well as the time history of several of the orbital elements. In the satellite trajectory plot, the green square indicates the initial position of the satellite, and the red diamond denotes the position of spacecraft at the end of the propagation interval. For the perturbed test case, the largest fluctuations in the orbital elements occur during the times when the NEO is close to perihelion.

rotating with the central and disturbing bodies. Along the line connecting these two bodies, the Hill Sphere radius is given by the positions of the collinear libration points $L_1$ and $L_2$ in the Circular Restricted Three Body Problem (CRTBP).

The CRTBP describes the motion of a third body due to the mutual gravitation of two other bodies: a primary body denoted $m_1$ and a secondary body denoted $m_2$. These bodies are constrained to follow circular orbits about their mutual barycenter, such that the distance between the two bodies is constant, $d$, and the line connecting them rotates at a constant angular velocity, $\Omega$. In the synodic frame rotating with the bodies, the libration points have fixed locations, since they are defined to be the positions where the combined gravitational attraction of $m_1$ and $m_2$ produces the exact centripetal acceleration needed to rotate in tandem with the bodies. There are five libration points in the CRTBP: three collinear points on the line connecting $m_1$ and $m_2$; and two equilateral points, one above and another below the connecting line. $L_1$ and $L_2$ are collinear libration points which straddle $m_2$; $L_1$ falls in between $m_1$ and $m_2$ and $L_2$ is on the far side of $m_2$ relative to $m_1$. The static positions of these points are found by setting to zero the acceleration and velocity terms in the CRTBP equations of motion expressed in the rotating frame. The collinear points are then given by the solutions to the quintic equation, which Szebehely showed could be expressed as a set of series expansions [24]:

$$r_{L_1} = d \left(\frac{\mu}{3}\right)^{1/3} \left[1 + \frac{1}{3}\left(\frac{\mu}{3}\right)^{1/3} - \frac{1}{9}\left(\frac{\mu}{3}\right)^{2/3} + \cdots \right], \tag{3.2}$$

$$r_{L_2} = d \left(\frac{\mu}{3}\right)^{1/3} \left[1 - \frac{1}{3}\left(\frac{\mu}{3}\right)^{1/3} - \frac{1}{9}\left(\frac{\mu}{3}\right)^{2/3} + \cdots \right], \tag{3.3}$$

where $d$ is the distance measured between $m_1$ and $m_2$ and $\mu = m_2/(m_1 + m_2)$ is the ratio of the secondary mass to the combined mass of the primary and secondary bodies. Note that the only difference between the first three terms in these series expansions is the sign of the second term. If $m_2 \ll m_1$ (clearly a valid assumption for the Sun-NEO system), then only the lowest order term of $(\mu/3)^{1/3}$ is significant. Dropping all higher order terms, the positions of the Libration points are

found to be equidistant from $m_2$, at a distance of

$$r_{\text{Hill}} = d \left( \frac{\mu}{3} \right)^{1/3},$$ (3.4)

called the Hill radius. If the orbit elements of $m_2$ are expressed in a frame centered on $m_1$, then the semi-major axis $a$ of the $m_2$ orbit can be substituted for $d$ in Equation 3.4. For the general case of $m_2$ following an ellipitical orbit about $m_1$, it was shown in [14] that the stability zone for $m_2$ is approximated by the Hill sphere radius evaluated at periapsis of its orbit:

$$r_{\text{Hill}} = a(1 - e) \left( \frac{\mu}{3} \right)^{1/3},$$ (3.5)

where $e$ is the orbit eccentricity.

In truth, the Hill sphere is not a sphere at all. The positions of the $L_1$ and $L_2$ libration points, $\pm r_{\text{Hill}}$ measured relative to the secondary mass position, define the intersections of a critical surface with the line connecting $m_1$ and $m_2$. The full surface is defined as the set of positions which evaluate to the same zero-velocity Jacobi constant as $L_1$ and $L_2$. The value of this constant is given by the Jacobi integral of the satellite motion as seen by a rotating frame centered on the secondary mass (i.e. the earlier defined $\mathcal{B}$ frame), defined in [13] as:

$$C = -\dot{x}^2 - \dot{y}^2 - \dot{z}^2 + \omega^2(3x^2 - z^2) + \frac{2Gm_2}{|\mathbf{r}|},$$ (3.6)

This equation can be expressed in dimensionless coordinates using a set of reduced units suggested by [10]. The time unit TU is defined to be the inverse of the angular velocity $(1/\Omega)$ and the distance unit DU to be the Hill radius $(r_{\text{Hill}})$. If the gravitation constant $(G)$ is set equal to unity, then the value of the mass unit MU can be solved for using Kepler's third law:

$$\begin{aligned}
\Omega^2 d^3 &= G(m_1 + m_2) \quad \text{[Dimensional Units]} \\
\frac{d^3}{r_{\text{Hill}}^3} &= \frac{m_1 + m_2}{\text{MU}} \quad \text{[Nondimensional Units]} \\
\text{MU} &= \frac{m_2}{3}
\end{aligned}$$ (3.7)

Substituting these reduced units into Equation 3.6 yields an expression for the Jacobi integral in dimensionless coordinates:

$$C = -\dot{x}^2 - \dot{y}^2 - \dot{z}^2 + 3x^2 - z^2 + \frac{6}{|\mathbf{r}|}. \tag{3.8}$$

By setting to zero the velocity terms in Equation 3.8 and plugging in the position of either of the $L_1$ or $L_2$ libration points, the critical zero-velocity value of the Jacobi constant is found to be 9 in dimensionless coordinates. The points that possess the same zero-velocity value of the Jacobi constant collectively define the boundary of a region within which any satellite possessing a Jacobi constant $\geq 9$ cannot escape. The intersection of this zero-velocity surface with the X-Y plane in the $\mathcal{B}$ frame is shown in Figure 3.3. Notice that the zero-velocity curve for $C = 9$ defines the largest region that is fully closed about the secondary body. This is why this zero-velocity surface is known as the critical surface; it represents the maximum region within which a satellite's motion can be bound to the secondary body.

### 3.2.2.1     Parametric study

For the NEO-Sun system, $m_1$ is the Sun and $m_2$ is the NEO. If the NEO is in a circular orbit of radius $d$ about the Sun, has a sphere-equivalent radius $R_\mathrm{N}$ and constant mass density $\rho$, and is much less massive than the Sun such that $\mu \approx M/M_\odot$, then Eq. 3.5 can be rewritten for the NEO-Sun system as

$$r_\mathrm{Hill} = dR_\mathrm{N} \left( \frac{4\pi}{9M_\odot} \rho \right)^{1/3}. \tag{3.9}$$

If the Hill radius is then normalized by the radius of the NEO, the resulting equation is independent of the NEO radius and linearly related to the Sun-NEO distance. A plot of this radius ratio is shown in Fig. 3.4.
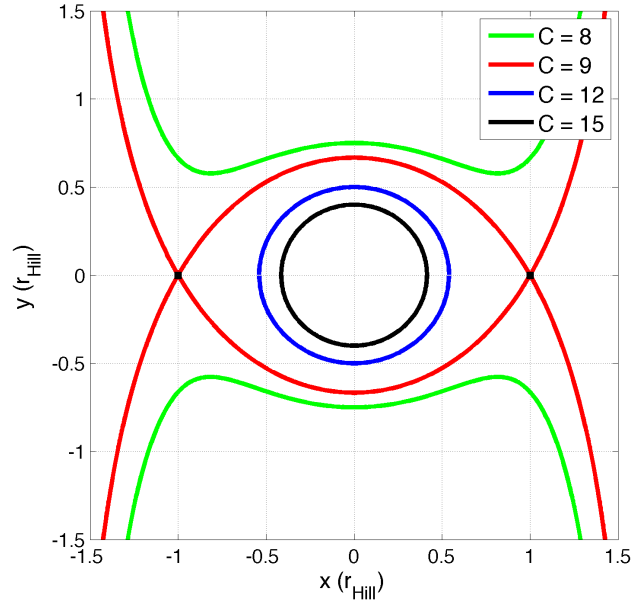
Figure 3.3: Plot of the zero-velocity curves for the Jacobi constant expressed in dimensionless coordinates. The curve for $C = 9$ bounds the largest region fully closed to the secondary body. The positions of the libration points $L_1$ and $L_2$ are shown as black squares on the plot.
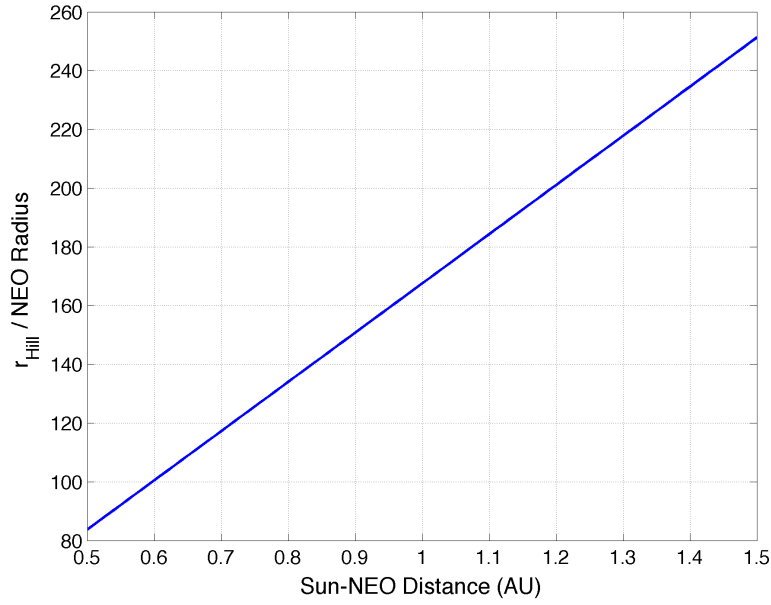


Figure 3.4: Plot of $r_{\text{Hill}}/R_{\text{N}}$ as computed by Eq. 3.9. Note that the NEO is assumed to have a constant mass density of $\rho = 2.0$ g/cc.

### 3.2.2.2    Numerical verification

To verify that a satellite within the NEO Hill sphere will remain bound to the NEO provided its Jacobi energy is higher than the critical value, a test was conducted using the NEO+satellite orbit model with the perturbations due to solar radiation pressure and a non-spherical NEO mass distribution deactivated. The NEO used for this test is defined to have the same orbit and physical parameters as were used in the SOI test in §3.2.1.2. Plugging the mass of the NEO and the NEO orbit periapsis distance into Equation 3.5, the Hill radius is found to be $\approx 42$ km. For both test cases, the satellite is initialized in a circular ecliptic orbit about the NEO. For the first test case, the size of this orbit is selected to be $a = 25.5$ km, which gives the satellite a Jacobi constant of $C = 9.0830$. Since the satellite Jacobi constant is greater than the critical value, it is expected that the satellite should remain bound to the NEO. For the second test case, the orbit size is $a = 27.5$ km, which initializes the satellite with a Jacobi constant of $C = 8.8003$. In this case the Jacobi constant is less than the critical value, so the satellite should escape from NEO orbit at some point in the propagation interval. Figure 3.5 shows that expectations were met for both test cases.

### 3.2.3    Maximum semi-major axis limit due to solar radiation pressure

In [21], a limit on the osculating semi-major axis for stability in the presence of a constant (in magnitude and direction) solar radiation pressure force is derived for a circular terminator orbit about a point mass:

$$a \leq \frac{\sqrt{3}}{4}\sqrt{\frac{4\pi c}{L_\odot}\frac{d^2 B \mu}{c_{\mathrm{R}}}} = a_{\mathrm{max}}. \tag{3.10}$$

Though this limit is derived in the context of a non-rotating and non-translating reference frame, it approaches the true limit for the general case of a small body in an elliptical orbit about the Sun, provided the solar radiation pressure force is strong [21].
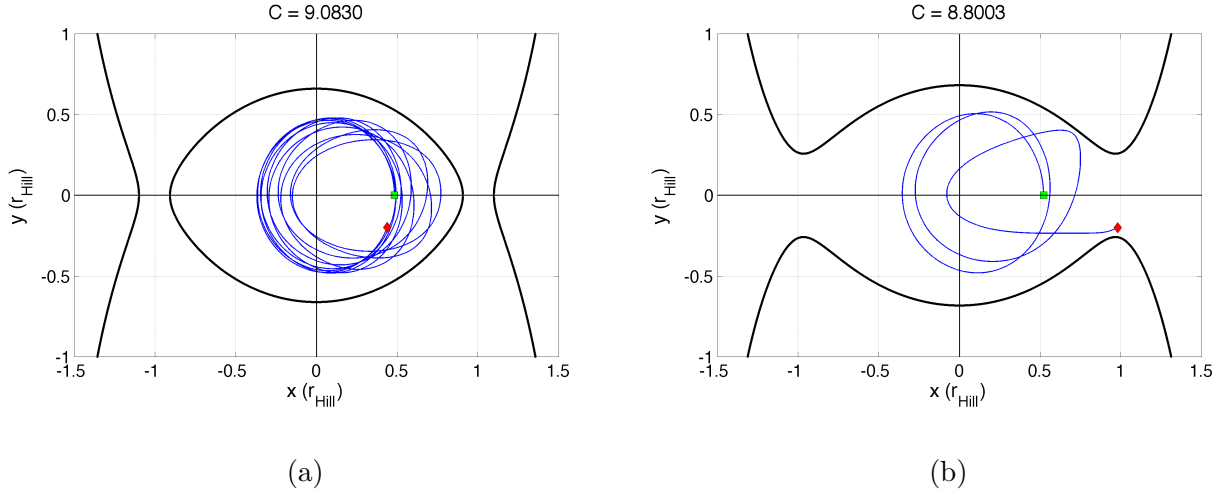
Figure 3.5: Results from the Hill radius test cases: (a) satellite with a Jacobi constant greater than the critical value; (b) satellite with a initial Jacobi constant less than the critical value. In each plot, the blue line denotes the trajectory of the satellite as viewed in the $\mathcal{B}$ frame, and the thick black line denotes the zero-velocity curve for the satellite Jacobi constant. Note that even though both satellites are initialized at positions within the Hill region, only the satellite possessing a Jacobi constant greater than the critical value remains bound to the NEO. The satellite with a Jacobi constant less than the critical value is able to escape because its zero velocity curve is open to free space.

### 3.2.3.1　　Parametric study

Assuming a NEO of sphere-equivalent radius $R_{\mathrm{N}}$ and constant mass density $\rho$, Equation 3.10 can be written as:

$$a_{\max} = \pi d \sqrt{\frac{cG}{L_{\odot}} \frac{B\rho R_{\mathrm{N}}^3}{c_{\mathrm{R}}}}. \tag{3.11}$$

To investigate the behavior of this equation, some characteristic values are chosen for several of the independent parameters. The reflectivity is set to 1 for a blackbody, and two mass/area ratio values are tested: one for an Orion-class spacecraft and another for an astronaut. The results are shown in Figure 3.6.

### 3.2.3.2　　Numerical Verification

To verify that a satellite in a terminator frozen orbit is stable up to and including the maximum semi-major axis limit derived for the solar radiation pressure perturbation, a test was conducted using the NEO+satellite orbit model with the perturbations due to third body gravity and a non-spherical NEO mass distribution deactivated. The NEO used for this test is defined to have the same orbit and physical parameters as were used in the SOI test in §3.2.1.2. The satellite is modeled as an Orion-class spacecraft, with a mass to area ratio of 400 and a reflectivity of 1 (blackbody). Using these parameters for the NEO and satellite and plugging in the periapsis distance of the NEO orbit, the value for $a_{\max}$ is computed from Equation 3.11 to be $\approx 13.2$ km. Four cases were executed for this test, each utilizing a larger semi-major axis than the previous case. For all cases, the orbit is designed to be a terminator frozen orbit with $\hat{\mathbf{h}}$ directed toward the Sun. Figure 3.7 shows the integrated trajectories as viewed from the $\mathcal{B}$ frame for each of the test cases. As expected, all orbits having a semi-major axis $\leq a_{\max}$ are stable, while the single case that had a semi-major axis $> a_{\max}$ escapes NEO orbit.

(a)



(b)
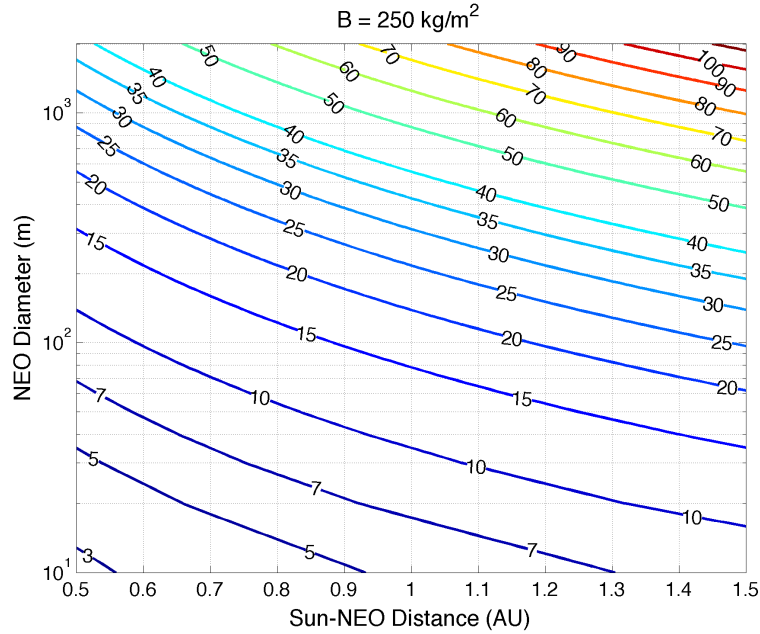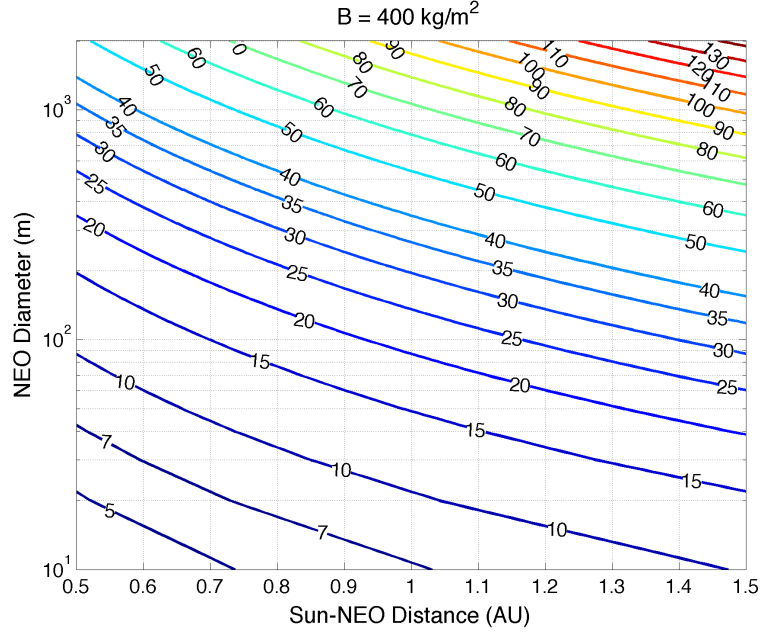
Figure 3.6: Contour plots of $a_{\max}/R_N$ as computed by Eq. 3.11 for (a) an Orion-class spacecraft and (b) an astronaut wearing a Shuttle class space suit. Note that the NEO is assumed to have a constant mass density of $\rho = 2.0$ g/cc and the reflectivity of the satellite (spacecraft or astronaut) is assumed to be 1 (blackbody). For a given NEO size and Sun-NEO distance, the maximum limit on the semi-major axis is smaller for an orbiting astronaut than for an Orion-class spacecraft because the astronaut's mass to area ratio is smaller than that of the spacecraft.
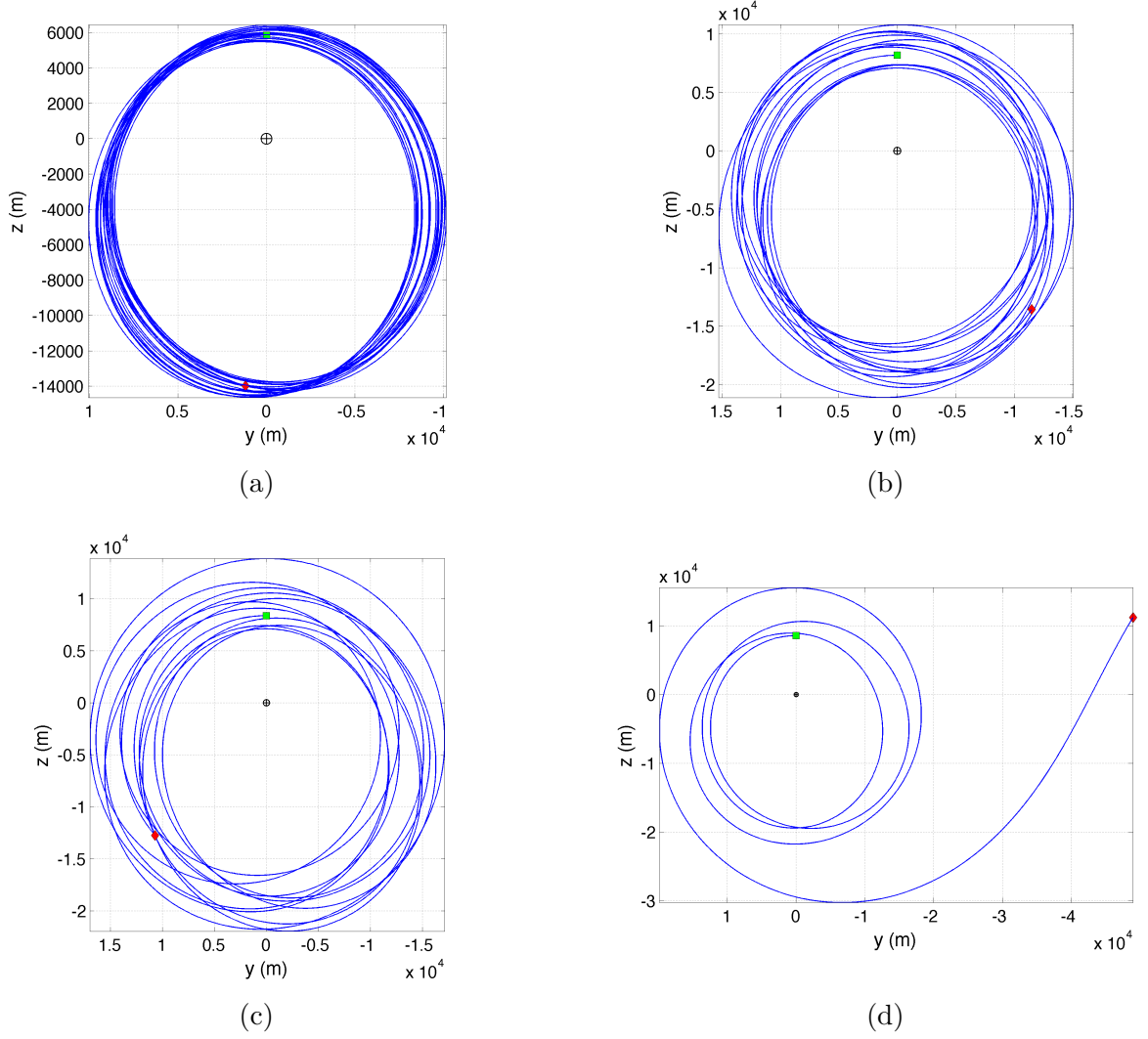
Figure 3.7: Results from the SRP test cases evaluating $a_{\mathrm{max}}$: (a) $a = 10$ km; (b) $a = 13$ km; (c) $a = a_{\mathrm{max}} \approx 13.2$ km; (d) $a = 13.5$ km. The trajectories are shown for the satellite in the $\mathcal{B}$ frame as seen by an observer on the negative x-axis (the Sun is behind the observer). The trajectories for cases (a) - (c) remain stable throughout the propagation interval (one full NEO orbit), though as $a$ approaches $a_{\mathrm{max}}$ the trajectory does begin to wander a bit in the terminator plane. The trajectory for case (d) escapes NEO orbit after 205 days.

### 3.2.4 Minimum semi-major axis limit due to NEO ellipticity

In [21], a minimum limit on the semi-major axis to guard against the destabilization of an orbit about a NEO due to the ellipticity of the NEO body is given as:

$$a > \frac{3}{2} r_{\text{res}} = a_{\min},$$ (3.12)

where

$$r_{\text{res}} = \left( \frac{P^2 \mu_{\text{N}}}{4\pi^2} \right)^{1/3}$$ (3.13)

is the resonance radius; the radius at which the gravitational acceleration due to NEO gravity is equal to the centripetal acceleration of its rotation. This minimum limit on the semi-major axis is empirically derived from the results of the numerical analysis conducted in [16] and shown in Figure 3.8. This figure depicts regions of stable and unstable orbits plotted against two parameters: $a_0^{2/3}$ and $I_z - I_x$; both normalized by the resonance radius. For convenience, we define the parameter $\chi$ to be equal to the second parameter in the plot:

$$\chi \equiv \frac{I_z - I_x}{r_{\text{res}}^2}.$$ (3.14)

$\chi$ can be thought of as a shape parameter, measuring the degree to which the shape of the NEO departs from a sphere. A $\chi$ value of 0 indicates that the NEO is a perfect sphere, and as $\chi$ increases the shape of the NEO becomes increasingly stretched along its $s$ axis.

#### 3.2.4.1 Parametric study

To study the behavior of Equation 3.12, the expression for the resonance radius in Equation 3.13 is rewritten for the case of a NEO of constant mass density $\rho$ and sphere-equivalent radius $R_{\text{N}}$:

$$r_{\text{res}} = R_{\text{N}} \left( \frac{G}{3\pi} P^2 \rho \right)^{1/3}.$$ (3.15)
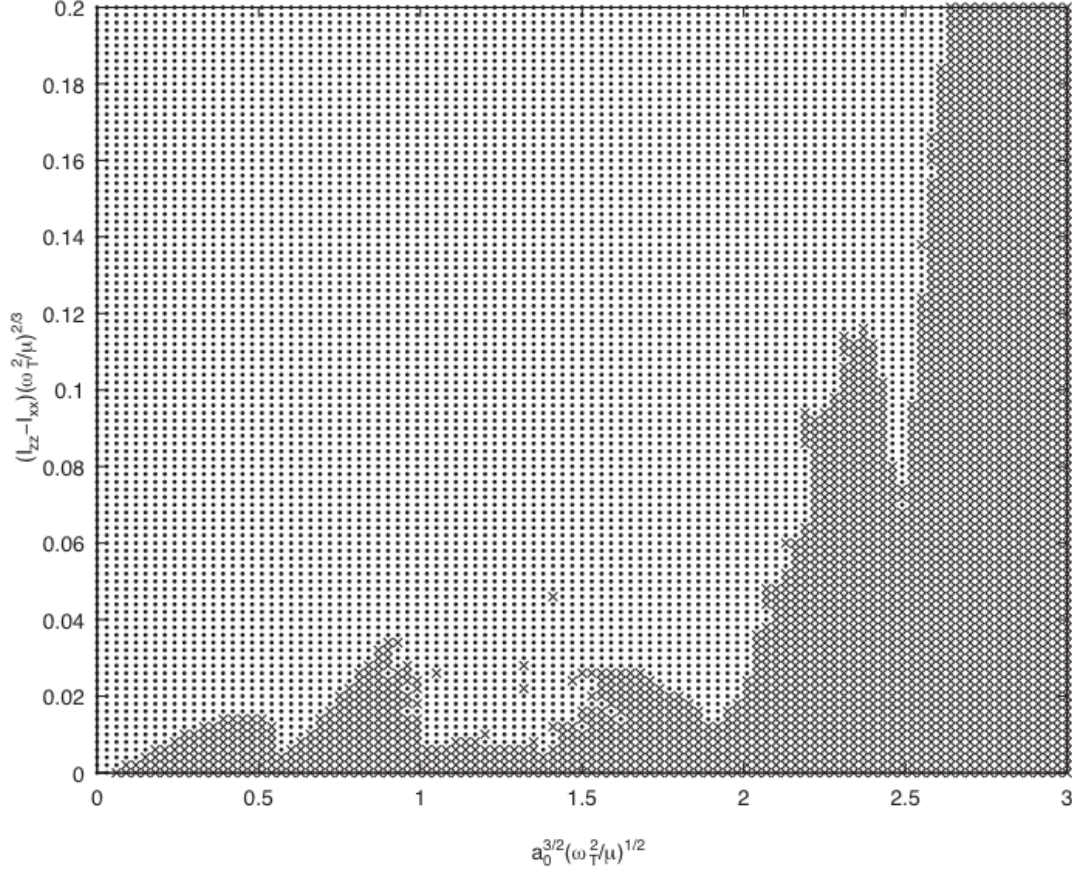
Figure 3.8: Regions of stable (denoted by [ × ]) and unstable (denoted by [ · ]) ecliptic circular orbits about a NEO having a $q : p$ ratio of 1. The x-axis units are $a_0^{3/2}$ and the y-axis units are $I_z - I_x$, both normalized by the resonance radius $r_{\text{res}}$. There appear to be regions of stability for nearly all values of $(a_0/r_{\text{res}})^{3/2}$, but the largest stable regions (covering the largest ranges of $(I_z - I_x)/r_{\text{res}}^2$) occur for $(a_0/r_{\text{res}})^{3/2} > 1.85 \approx (1.5)^{3/2}$. Note that this empirically-derived boundary is the origin of the minimum limit on the satellite orbit semi-major axis given in Equation 3.12. The figure is taken from [16].

When the equation for the resonance radius is expressed in this form, it is clear that the value of the resonance radius depends on only two free parameters (assuming the mass density is fixed): the NEO sphere-equivalent radius and the rotation period. Note that there is no dependence on the actual shape of the NEO, so that the resonance radius can be the same for NEOs of any shape provided their sphere-equivalent radii (and therefore their masses) are equal. Since $a_{\text{min}}$ is directly proportional to $r_{\text{res}}$, these dependencies also apply to $a_{\text{min}}$. The qualitative dependencies of $a_{\text{min}}$ on the rotation period and size of the NEO are given in Table 3.1.

By substituting Equation 3.15 into Equation 3.12 and then dividing by the NEO sphere-equivalent radius, the ratio of $a_{\text{min}}$ to $R_{\text{N}}$ is found to be directly proportional to $P^{2/3}$. A plot of this distance ratio versus the NEO rotation period is shown in Figure 3.9.

Because the $\chi$ parameter is a function of the body moments of inertia, the shape of the NEO matters when computing this quantity. The shape of an ellipsoid is fully described by the ratio of its $s$ axis to its $q$ axis, $s : q$, provided the ratio of the $q$ and $p$ axes is constrained to unity. Assuming the NEO to be orbited has such a shape, then its mass is given by

$$M = \rho \frac{4}{3} \pi \frac{s^3}{(s : q)^2},$$

where

$$\frac{s}{(s : q)^{2/3}} = R_{\text{N}}$$

is the relationship between the ellipsoid dimensions and the sphere-equivalent radius. Substituting this expression for the NEO mass into Equation 3.13 and the replacing $I_z$ and $I_x$ in Equation 3.14 with the expressions from Equation 2.10 yields a new expression for $\chi$:

$$\chi = \frac{1}{5} \left( \frac{3\pi(s : q)^2}{G\rho P^2} \right)^{2/3} \left( 1 - \frac{1}{(s : q)^2} \right). \tag{3.16}$$

Inspection of Equation 3.16 reveals that the value of $\chi$ is independent of the size of the NEO $s$ axis and dependent only on the parameters $P$ and $s : q$. Thus, $\chi$ can have the same value for NEOs of various sizes provided $s : q$ and $P$ are held constant between them. To demonstrate the quantitative dependence of $\chi$ on these free parameters, contours of equal $\chi$ are plotted against

representative ranges of $P$ and $s : q$ in Figure 3.9. A summary of the qualitative dependencies of $\chi$ on these parameters is given in Table 3.1.

Table 3.1: Dependence of $a_{\min}$ and $\chi$ on NEO parameters

| Increasing... | $a_{\min}$ | $\chi$ |
|:---:|:---:|:---:|
| $P$ | Increases | Decreases |
| $s : q^{\dagger}$ | Constant | Increases |
| $s^{\ddagger}$ | Increases | Constant |

$^{\dagger}$Assumes total NEO mass is held constant.
$^{\ddagger}$Assumes the $s : q$ ratio is held constant.

### 3.2.4.2  Numerical verification

To verify that a satellite's orbit about a NEO is destabilized if the semi-major axis is less than the minimum threshold set to avoid ellipticity effects, a test was conducted using the NEO+satellite orbit model with the perturbations due to third body gravity and solar radiation pressure deactivated. The NEO used for this test is defined to have the same orbit parameters and mass density as were used in the SOI test in §3.2.1.2. The NEO body is modeled as an ellipsoid with semi-principal axes $[s, q, p] = [500, 300, 300]$ m, and is assumed to be rotating uniformly about its polar axis (oriented 45° in right ascension and obliquity relative to the non-rotating $\mathcal{N}'$ frame) with a period of 12 hours. Using these parameters for the NEO, the value of $a_{\min}$ is computed from Equation 3.12 to be $\approx 1.59$ km. The satellite is designed to have an ecliptic circular orbit, with a semi-major axis less than $a_{\min}$ in the first case and a semi-major axis greater than $a_{\min}$ in the second case. As expected, the first orbit destabilizes after a short period, while the second orbit remains stable for the entire propagation period. The integrated trajectories for both test cases are shown in Figure 3.10.
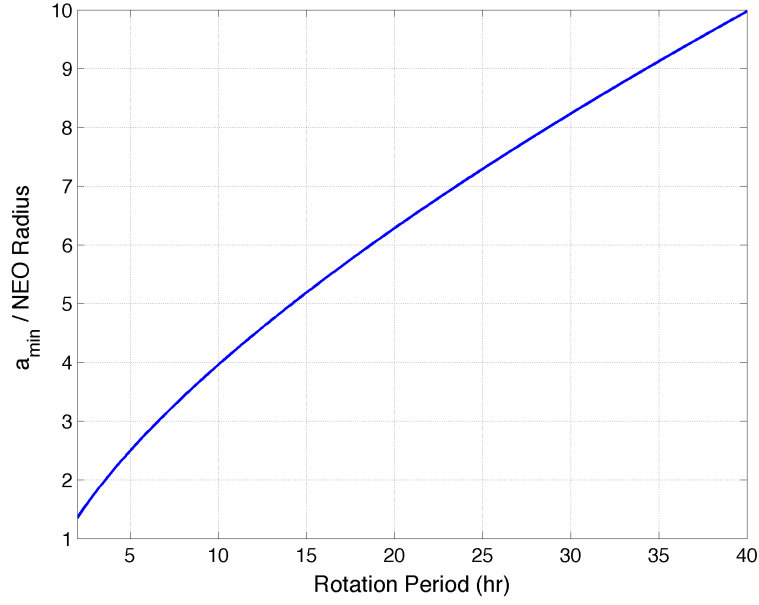
(a)
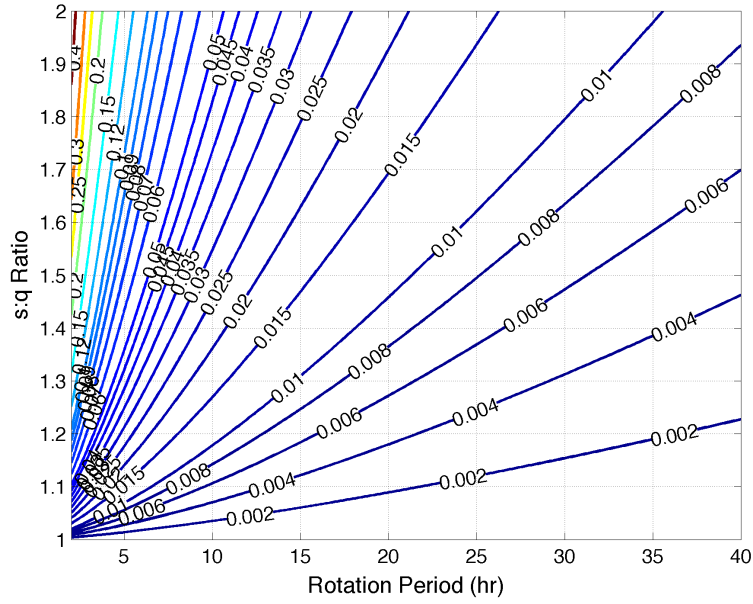


(b)

Figure 3.9: Plots of (a) $a_{\min}/R_{\mathrm{N}}$ as computed by Equations 3.12 and 3.15; and (b) equal contours of $\chi$ as computed by Equation 3.16. Note that the NEO is assumed to have a constant mass density of $\rho = 2.0$ g/cc.
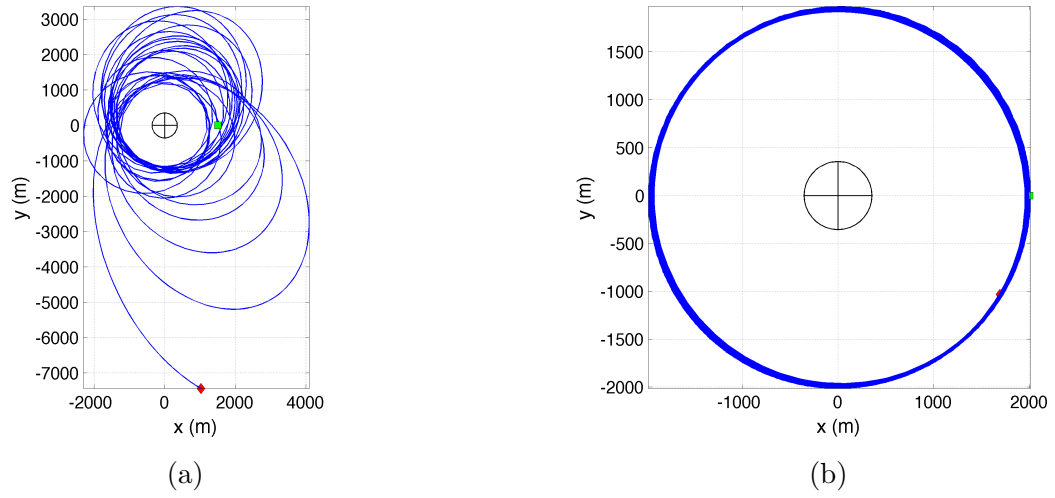
Figure 3.10: Results from the mass distribution test cases evaluating $a_{\min}$: (a) $a = 1.5$ km $< a_{\min}$; (b) $a = 2.0$ km $> a_{\min}$. The NEO is an ellipsoid with semi-principal axes $[s, p, q] = [500, 300, 300]$ m, and is plotted in the figures as its equivalent sphere (sphere having the same volume as the ellipsoid). The trajectory for case (a) escapes NEO orbit after 32 days.

## 3.3    Numerical Studies

Using the NEO+satellite orbit model described in Chapter 2 and the fixed NEO and Orion parameters listed in Table 2.1, several numerical studies were conducted with the objective to answer some of the most pressing questions regarding the feasibility and viability of orbiting the target body for a manned mission to a NEO.

### 3.3.1    How small of a NEO can be orbited?

It is a commonly held belief that most (if not all) small bodies in the solar system do not possess enough mass to be orbited by another body, such as a spacecraft. Of course, in a system isolated from any other attractive or disturbing forces, two bodies will orbit their mutual barycenter solely under the influence of their mutual gravitational attraction. This two-body assumption is often used to describe the dynamics of the system if the masses of the bodies are large, since the magnitude of the attractive force between them is directly proportional to the product of their masses. However, as the masses of the bodies get smaller, it becomes easier for the two-body motion to be disrupted by perturbative forces, such as those due to third body gravitation and solar radiation pressure. Typically, the strongest force perturbing two body dynamics in the NEO environment is solar radiation pressure, which exerts an acceleration on the satellite proportional to (among other parameters) $B^{-1}$, the inverse of the satellite mass to area ratio. Because an Orion-class spacecraft possesses a mass to area ratio an order of magnitude larger than typical unmanned satellites, it is less susceptible to the destabilizing effects of solar radiation pressure. This, in principle, would allow Orion to maintain orbit stability about NEOs at larger distances than those achievable by other spacecraft, but it also opens up the possibility for Orion to orbit about smaller NEOs than those that could be orbited by smaller, less massive satellites.

To investigate how small of a NEO an Orion-class spacecraft could stably orbit, simulations were conducted sequentially against NEOs of progressively smaller size. In each case, the spacecraft state was initialized to establish a terminator frozen orbit of size $a = a_{\max}$. The purpose of

maximizing the orbit size was to minimize the effect of the non-spherical mass distribution on the orbit. It was assumed that if the spacecraft couldn't stably orbit at the maximum distance permitted by the solar radiation pressure perturbation, then it probably couldn't establish a stable orbit at a distance closer to the NEO where the effects of the mass distribution would be greater. The shape distribution study of asteroid families in [23] found that a $s : q$ ratio of $\approx 1.2$ is the most common in the observable asteroid population, so each NEO is constrained to have this $s : q$ ratio and $q : p = 1$. Finally, the NEO rotation period for each simulation was set to 15 hours, both because the study in [5] indicated that targets for manned missions should have $P > 10$ hours, and also because the range of the effects due to the non-spherical distribution is extended for a longer NEO rotation period.

The results of the simulations showed that Orion-class spacecraft could establish a stable orbit about every NEO tested, including the smallest having semi-principal axes [10, 8.3, 8.3] m. Though the results seem to indicate that even smaller NEOs could theoretically be orbited by an Orion-class spacecraft, nothing smaller was tested for two reasons: (1) it seems unlikely that a manned mission would be planned to a NEO much smaller than $\approx 20$ m in diameter; and (2) for smaller NEOs the mass would begin to approach the mass of the Orion-class spacecraft and would therefore increasingly necessitate the inclusion of the acceleration of the spacecraft on the NEO in the orbit model. Admittedly, the second reason is probably not as strong an argument for not testing somewhat smaller NEOs, since the smallest NEO tested still has a mass several orders of magnitude larger than the mass of an Orion-class spacecraft, such that the system center of mass is only offset 25 cm from the NEO center of mass for the largest stable orbit ($a = a_{\max}$). The critical case would be for a NEO having a mass equal to that of an Orion-class spacecraft, which is found to be met for a NEO of sphere-equivalent radius $R_{\mathrm{N}} \approx 3$ m, assuming a constant mass density of 2.0 g/cc for the NEO.

Since an Orion-class spacecraft was found to be able to achieve orbit about the smallest NEO at the maximum distance permitted by the solar radiation pressure perturbation, several other simulations were executed in order to determine how much closer the spacecraft could get to

the NEO and still maintain a stable orbit. One other simulation was also run to verify that the spacecraft would escape NEO orbit if placed into an initial orbit having $a > a_{\mathrm{max}} \approx 71$ m. The integrated trajectories from these simulations are shown in Figure 3.11. The spacecraft initialized outside of $a_{\mathrm{max}}$ escapes NEO orbit as expected, but contrary to expectations the spacecraft orbits established inside of $a_{\mathrm{min}} \approx 46$ m remain relatively stable over the full NEO orbit. The orbit initialized at $a = 25$ m does eventually impact the NEO surface, but only after a period of 200 days, which is significantly longer than the likely duration of a manned mission to the NEO.

The $\chi$ parameter for this NEO ($s : q = 1.2$, $P = 15$ hr) is calculated to be 0.006676, which in Figure 3.8 is found to correspond to stable orbits for nearly all values of $(a/r_{\mathrm{res}})^{3/2}$. This explains why orbits below $a_{\mathrm{min}}$ remained stable for this NEO: the perturbation due to the NEO ellipticity was too weak to destabilize them. Since the value of $\chi$ increases with a decreasing rotation period or increasing $s : q$ ratio, these NEO parameters were adjusted to see whether the Orion-class spacecraft orbits below $a_{\mathrm{min}}$ would remain stable.

### 3.3.1.1    Does the shape matter?

To investigate whether a more elongated small NEO could destabilize the stable low altitude orbits found in the previous section, the $s : q$ ratio of the small NEO was increased to 2.0. The dimension of the $s$ axis was solved for given the constraint that the total volume of the new NEO must equal that of the previous NEO modeled in §3.3.1:

$$s' = (s_0 q_0 p_0 (s : q)^2)^{1/3} = 14.0197 \text{ m}.$$

All other physical parameters of the NEO (rotation period, mass density, etc...) were left unchanged. Because the total volume, and therefore the total mass, of the NEO was held fixed, the value of $a_{\mathrm{min}}$ was held constant at $\approx 46$ m. However, the larger $s : q$ ratio causes the $\chi$ value to increase to 0.031635. Figure 3.8 shows that there are very few stable orbits below the $a_{\mathrm{min}}$ threshold for this value of $\chi$. To confirm this expectation, a simulation was conducted for an Orion-class spacecraft initialized in a terminator frozen orbit of size $a = 35$ m about the elongated NEO. After a period
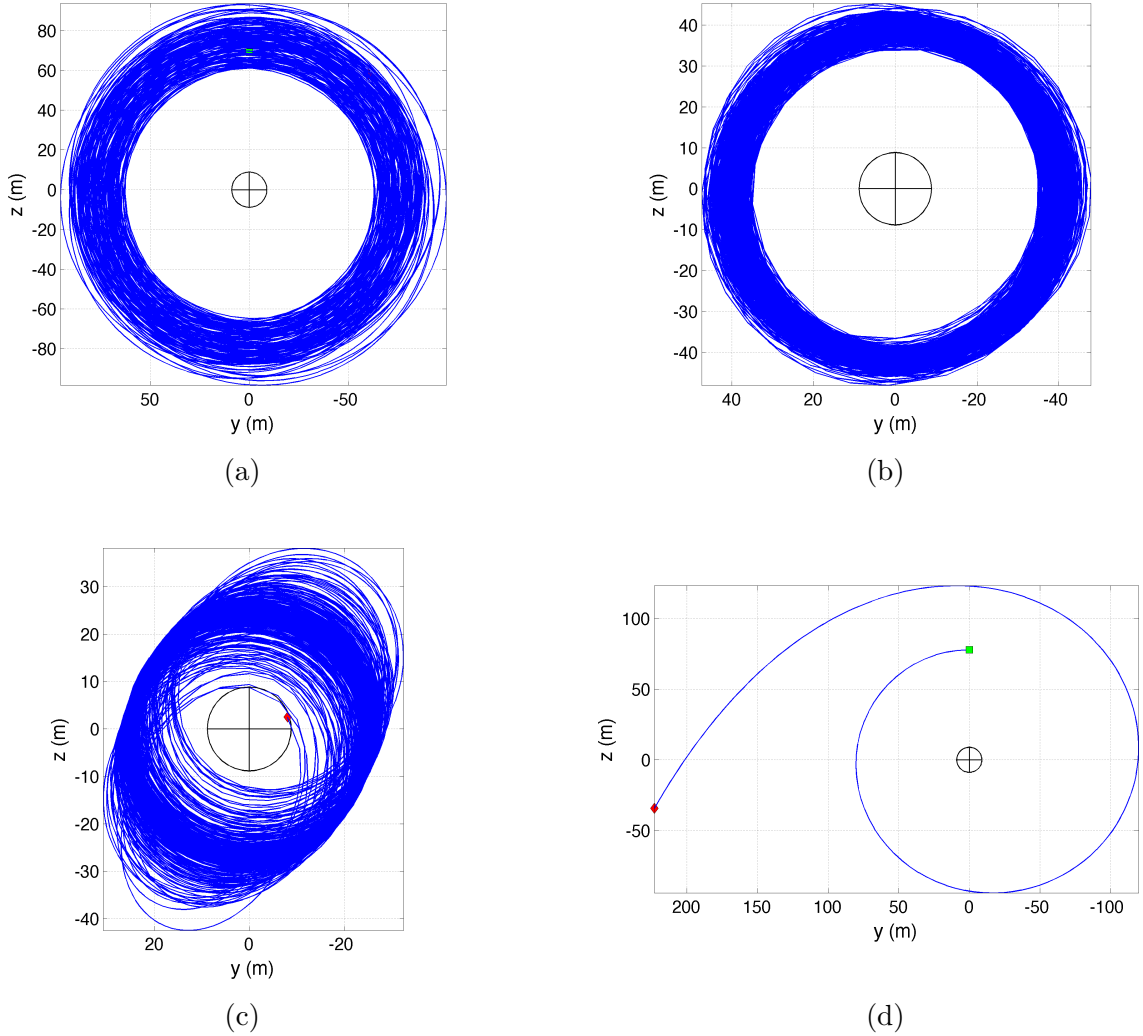
Figure 3.11: Integrated trajectories for an Orion-class spacecraft orbiting a small NEO ($[s, q, p] =$ $[10.0, 8.3, 8.3]$ m): (a) $a = a_{\max} \approx 71$ m; (b) $a = 40$ m $< a_{\min}$; (c) $a = 25$ m $<< a_{\min}$; (d) $a = 80$ m $> a_{\max}$. Because $\chi \approx 0.0067$ is so low for this NEO ($P = 15$ hr, $s : q = 1.2$), the ellipticity effects due to the non-spherical mass distribution of the NEO are weak. For case (c), the spacecraft orbits just slightly above the NEO surface and does eventually impact, but only after orbiting the NEO for a period of 196 days. In contrast to the mass distribution perturbation, the perturbation due to solar radiation pressure is found to have the ability to destabilize the orbit quite quickly. Increasing the semi-major axis just slightly above the maximum stability limit results in escape from NEO orbit in less than 7 days.

of 20 days, the orbit begins to destabilize, and after 60 days the spacecraft escapes NEO orbit.

This result indicates that the $a_{\min}$ threshold for orbits about a NEO becomes more firm as the NEO becomes more elongated (higher $s : q$ ratio). Thus, the interesting $a_{\max}$ to NEO surface orbit stability observed for the first small NEO tested appears to be a consequence of its rounder shape.



Figure 3.12: Results from the simulation of an Orion-class spacecraft orbiting a small NEO ($[s, q, p] = [14.0197, 7.00985, 7.00985]$ m) in a terminator frozen orbit initialized with $a = 35$ m $< a_{\min}$. The ellipticity effects, which are stronger for this NEO due to its more elongated shape, begin to destabilize the orbit after only 20 days and lead to escape after 60 days.

### 3.3.1.2   Does the rotation period matter?

The other NEO parameter that can be adjusted to increase the $\chi$ value for the NEO is the rotation period. $\chi$ is inversely proportional to $P^{4/3}$, so decreasing $P$ results in increasing $\chi$. The rotation period of the NEO is set to 10 hours, which was given in [5] as the shortest period acceptable for the target of a manned mission to a NEO. All other values for the physical parameters of the NEO were held constant from §3.3.1. The shorter rotation period for this NEO leads to a smaller value for the minimum semi-major axis threshold – $a_{\min} \approx 35$ m – and a larger value for the shape parameter – $\chi = 0.011463$. These new values imply that the threshold orbit size for guarding against ellipticity effects is lower for this NEO, but at the same time the strength of those

effects within the threshold distance are stronger than they were for the previous small NEO. To test this behavior, an Orion-class spacecraft is initialized in a terminator frozen orbit with the same semi-major axis as the smallest orbit tested in §3.3.1. The results of the simulation (see Figure 3.13) show that this low altitude orbit impacts the surface much more quickly for the more rapidly rotating NEO.

In summary, decreasing the rotation period of the NEO has both a stabilizing and destabilizing effect on the satellite orbit. Because $a_{\min}$ is smaller for NEOs with a faster rotation, satellites can orbit closer to these bodies without experiencing the destabilizing effects due to the body ellipticity. However, if the satellite orbit falls below the $a_{\min}$ threshold, then the faster rotation enhances the strength of ellipticity effects and can destabilize the orbit more quickly.
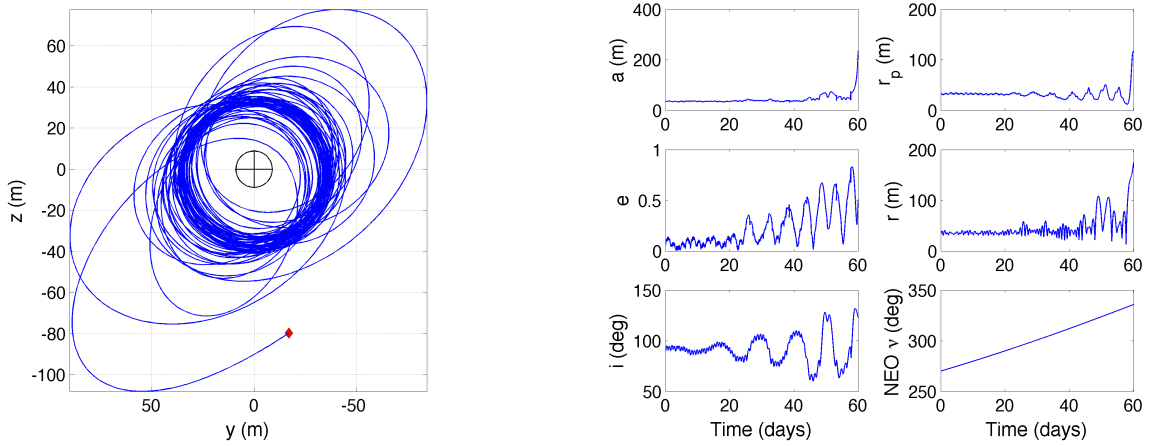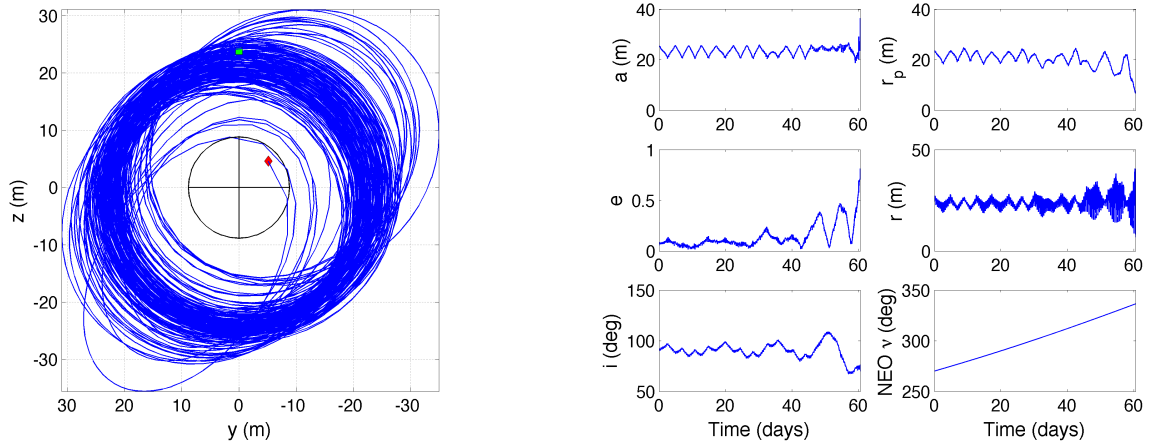


Figure 3.13: Results from the simulation of an Orion-class spacecraft orbiting a small NEO ($[s, q, p] = [10, 8.3, 8.3]$ m) in a terminator frozen orbit initialized with $a = 25$ m $< a_{\min}$. The ellipticity effects, which are stronger for this NEO due to its shorter rotation period, cause the spacecraft to impact the surface after 60 days.

### 3.3.2    Are there NEOs that Orion cannot orbit?

The previous studies have shown that a wide range of NEOs could potentially be orbited by an Orion-class spacecraft, which begs the question: are there any NEOs which cannot be orbited? Theoretically, the answer to this question is yes, provided the parameters of the system

are configured such that the value of $a_{\min}$ exceeds that of $a_{\max}$. Figure 3.14 shows contours of $a_{\max}/a_{\min}$ plotted for a wide range of rotation periods and NEO diameters. The plot clearly shows that NEOs with long rotation periods can have $a_{\min} > a_{\max}$, and that the rotation period at which this threshold is crossed is shorter for smaller NEOs and longer for larger NEOs.

Recall that the study in §3.3.1 showed that the degree to which the the $a_{\min}$ constraint is *firm* depends on the shape of the NEO. For rounder, more spherical NEOs, orbits having a semi-major axis smaller than the minimum threshold can remain stable in the presence of ellipticity effects. Thus, provided that the mass and rotation period of a NEO cause it to fall in the region where $a_{\min} > a_{\max}$, it is possible that this NEO could still be stably orbited if its shape is not too elongated. To test this hypothesis, a numerical simulation was run for an Orion-class spacecraft orbiting a small, very slowly rotating NEO. The NEO $s : q$ ratio was initially set to 4.0 to demonstrate that no orbits were possible, and then decreased to 3.0 to show that a rounder NEO could be orbited provided all other parameters were held constant. The results of these simulations are shown in Figure 3.15.

### 3.3.3    Why terminator frozen orbits?

The results of the previous study showed that a terminator frozen orbit can be long-term stable provided that the semi-major axis falls within the maximum and minimum limits for stability. However, given that an Orion-class spacecraft has such a high mass to area ratio compared to other spacecraft, it might seem reasonable that other types of orbits could also be stable in the NEO environment. In particular, one of simplest alternatives would be a circular orbit at an arbitrary orientation relative to the NEO. A numerical simulation was conducted to test the viability of such an orbit, which was initialized to have a semi-major axis of 3 km, an inclination of 45° relative to the ecliptic plane, and an azimuth of 45° relative to the terminator plane. The NEO is modeled as a uniformly rotating ellipsoid with $s : q$ ratio of 2.0, $s$ axis of 200 m, and a rotation period of 15 hours. The simulation results for the circular orbit propagation are shown in Figure 3.16 along with the results for a terminator frozen orbit having the same initial semi-major axis. The
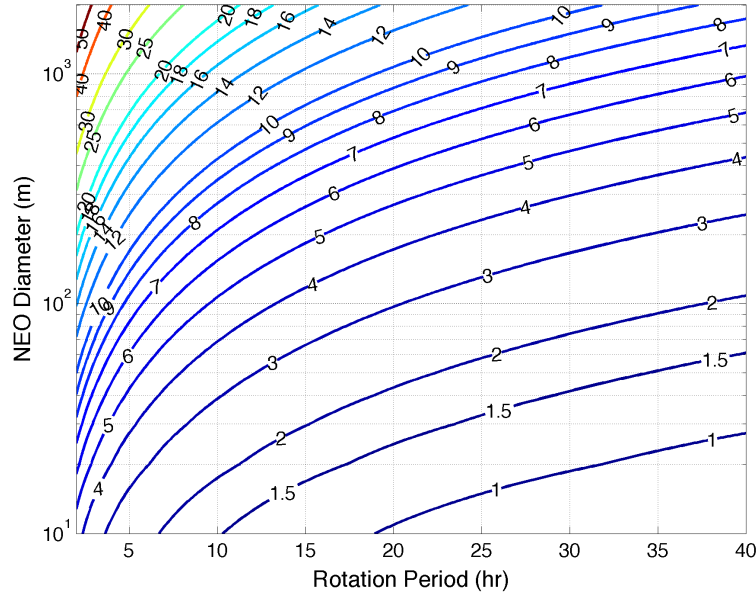
Figure 3.14: Contours of $a_{\max}/a_{\min}$. The plot shows that NEOs with a small diameter and a long rotation period can have a value for this ratio of less than one. In principle, these NEOs cannot be orbited by Orion, though depending on the shape of the NEO, and thus the value of $\chi$, the ellipticity perturbation may be weak enough to allow stability over extended periods. The assumptions used to produce this plot are: the NEO has a constant mass density of $\rho = 2.0$ g/cc; $a_{\max}$ is evaluated at the perihelion distance of the heliocentric orbit specified in Table 2.1; and the satellite is an Orion-class spacecraft with $B = 400$ kg/m$^2$.
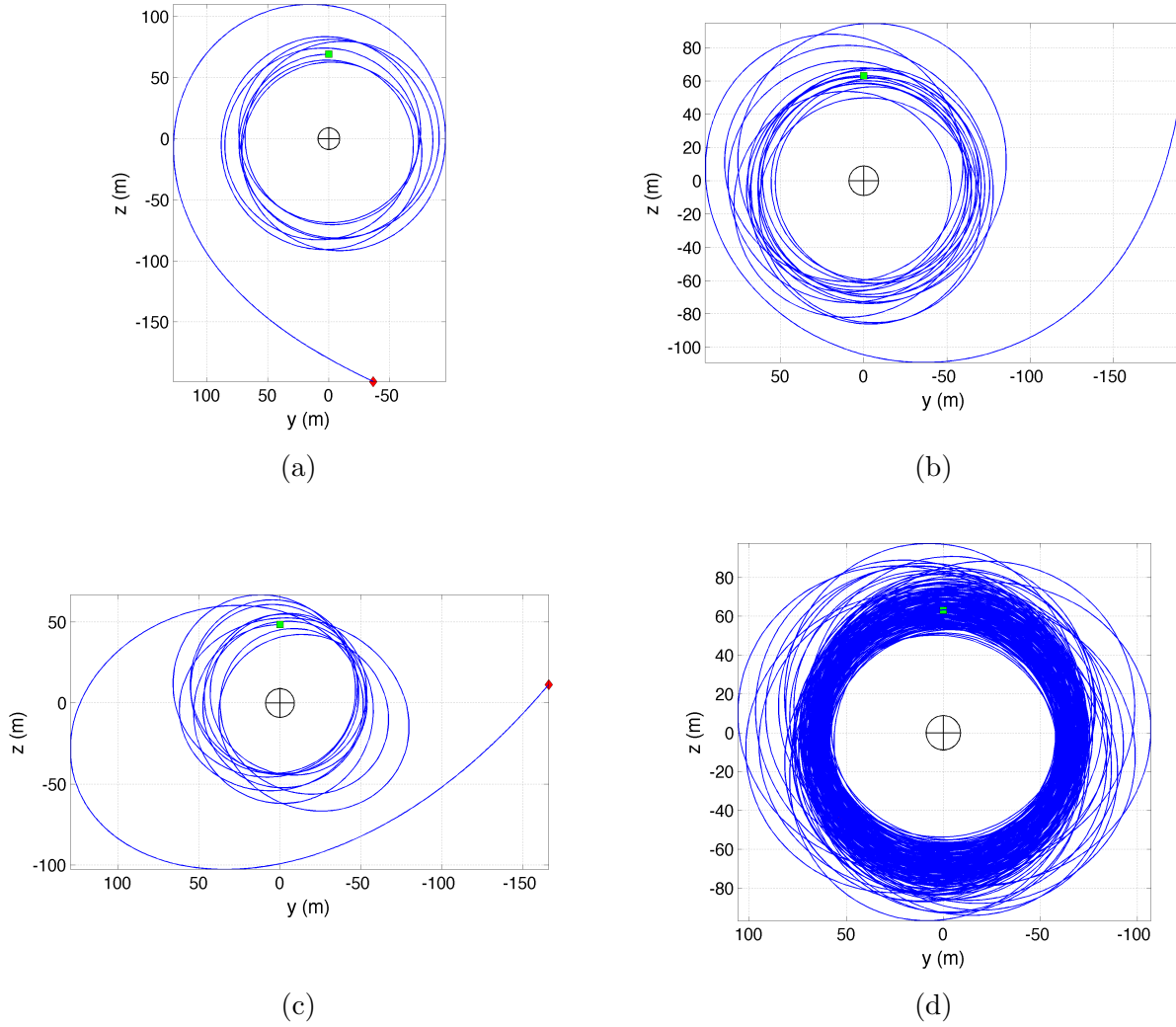
Figure 3.15: Integrated trajectories for an Orion-class spacecraft orbiting a small, slowly rotating NEO: (a) $s : q = 4.0$, $a = a_{\max}$; (b) $s : q = 4.0$, $a = 65$ m; (c) $s : q = 4.0$, $a = 50$ m; (d) $s : q = 3.0$, $a = 65$ m. In all cases, the $s$ axis dimension of the NEO is solved for given the ellipsoid $s : q$ ratio and the constraint that the total volume equal that of the NEO from §3.3.1. The rotation period is 35 hr, which causes $a_{\min}$ to grow beyond $a_{\max}$ consistent with Figure 3.14. For cases (a) - (c), $\chi = 0.032197$, and for (d) $\chi = 0.020802$. As shown in panels (a) - (c), the NEO with $s : q = 4.0$ cannot be orbited by Orion at any distance. However, (d) shows that the NEO with $s : q = 3.0$ can be orbited despite the fact that $a_{\min} > a_{\max}$. This is because the value of $\chi$, and thus the strength of the ellipticity perturbation, is low enough to permit the orbit to remain stable over the period of one NEO orbit about the Sun.

spacecraft initialized in the circular orbit follows a highly perturbed but bounded trajectory until it finally escapes 146 days after the propagation epoch, while the terminator frozen orbit remains stable for the full cycle of the NEO orbit. While the trajectory for the initial circular orbit does remain bounded for a period likely much greater than the duration of any manned mission, the rapid variation of its osculating orbit elements would not be desirable for such a mission. The terminator frozen orbit, on the other hand, provides a stable trajectory useful for both conducting scientific studies of the NEO as well as for staging astronaut EVAs to the NEO surface.

Therefore, owing partly to Orion's high mass to area ratio, it is possible to achieve and temporarily maintain a non-frozen orbit about a small body. However, while this orbit can remain bound to the NEO for a period of time, its osculating elements will vary rapidly and therefore it is not be an ideal candidate for meeting the objectives of a manned mission.

In §2.8 another family of frozen orbits, called ecliptic frozen orbits, were introduced and a procedure for creating them was provided. To this point, however, this family of orbits has been excluded from all of the simulation test cases in favor of terminator frozen orbits. To understand why this has been the case, it is important to consider how each family of orbits adjust as the strength of the solar radiation pressure perturbation varies. The parameter $\psi$ is used to describe the strength of this perturbation and is given by:

$$
\begin{aligned}
\Lambda &= \frac{3L_\odot}{8B\pi c}\sqrt{\frac{a}{P\mu_{\mathrm{N}}\mu_\odot}}, \\
\psi &= \tan^{-1}\Lambda.
\end{aligned}
\tag{3.17}
$$

Equation 3.17 shows that $\psi$ is a function of both NEO and satellite parameters. Since the orbit of the NEO and the mass to area ratio of the satellite have been fixed in our model, the only parameters which can be adjusted to change the value of $\psi$ are the satellite orbit semi-major axis $a$ and the NEO gravitational parameter $\mu_{\mathrm{N}}$. Since $\psi$ is proportional to $\sqrt{a}$ and inversely proportional to $\sqrt{\mu_{\mathrm{N}}}$, $\psi$ grows larger for larger orbits about the NEO or less massive (i.e. smaller sized) NEOs. Given that the value of $\Lambda$ can only vary between 0 and 1, the solar radiation pressure perturbation grows weak as $\psi \to 0$ and strong as $\psi \to \pi/2$. In §2.8, the formulas for computing the frozen orbit
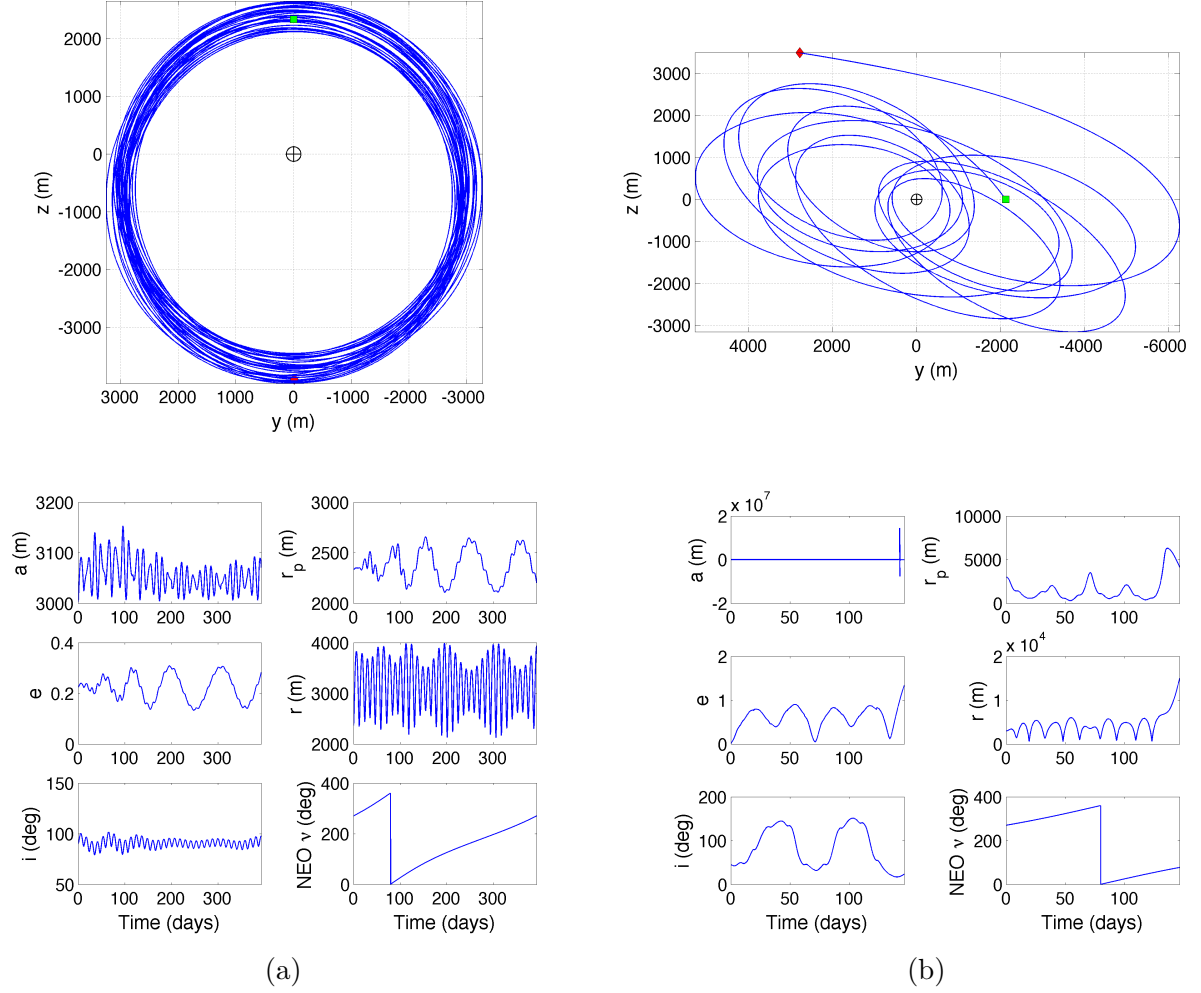
Figure 3.16: Integrated trajectories for an Orion-class spacecraft orbiting about a medium NEO ($[s, q, p] = [200, 100, 100]$ m): (a) terminator frozen orbit with $\hat{\mathbf{h}}$ directed toward the Sun; (b) circular orbit rotated 45° out of the terminator plane and inclined 45° above the ecliptic plane. Both orbits are initialized with a semi-major axis of $a = 3$ km. The spacecraft in the terminator frozen orbit is found to remain bound and stable throughout the propagation interval, while the spacecraft in the inclined circular orbit escapes after 146 days.

eccentricity from the $\psi$ parameter were given as:

$$
e = \begin{cases} \cos\psi, & \text{terminator frozen orbit} \\ \sin\psi, & \text{ecliptic frozen orbit} \end{cases} \tag{3.18}
$$

As the strength of the solar radiation pressure perturbation increases, a terminator frozen orbit approaches a circular orbit while an ecliptic frozen orbit tends toward a parabolic trajectory. For this reason, ecliptic frozen orbits are not preferred for strongly perturbed situations, since in these situations they will be highly eccentric with a low altitude for periapsis. This is undesirable because the orbit can become destabilized during periapsis passage if the NEO mass distribution is not spherical. Figures 3.17 and 3.18 show simulation results for prograde and retrograde orbits modeled about a medium-sized NEO characterized by the parameters $s : q = 2$, $s \approx 476$ m and $P = 15$ hours. Both orbit types are stable if only the perturbation due to solar radiation pressure is activated, but once the other perturbations are activated that stability is lost almost immediately. The retrograde ecliptic frozen orbit does seem to show a higher resilience to the influence of the other perturbations, however its osculating elements still vary too much to be considered a suitable candidate for a manned mission.

(a)

(b)

Figure 3.17: Prograde ecliptic frozen orbit trajectory for an Orion-class spacecraft orbiting a medium-sized NEO ($[s, q, p] = [476.22032, 238.11016, 238.11016]$ m): (a) motion modeled with only the solar radiation pressure perturbation active, and (b) motion modeled with all perturbations active. The orbit is initialized with a semi-major axis of $a = 3$ km, which sets a periapsis radius of $\approx 700$ m. Since periapsis for the frozen orbit lies below the limit for guarding against ellipticity effects ($a_{\min} \approx 1.55$ km), the motion is significantly perturbed by the non-spherical mass distribution during each periapsis passage. The orbit quickly destabilizes, and results in surface impact after 18 days.
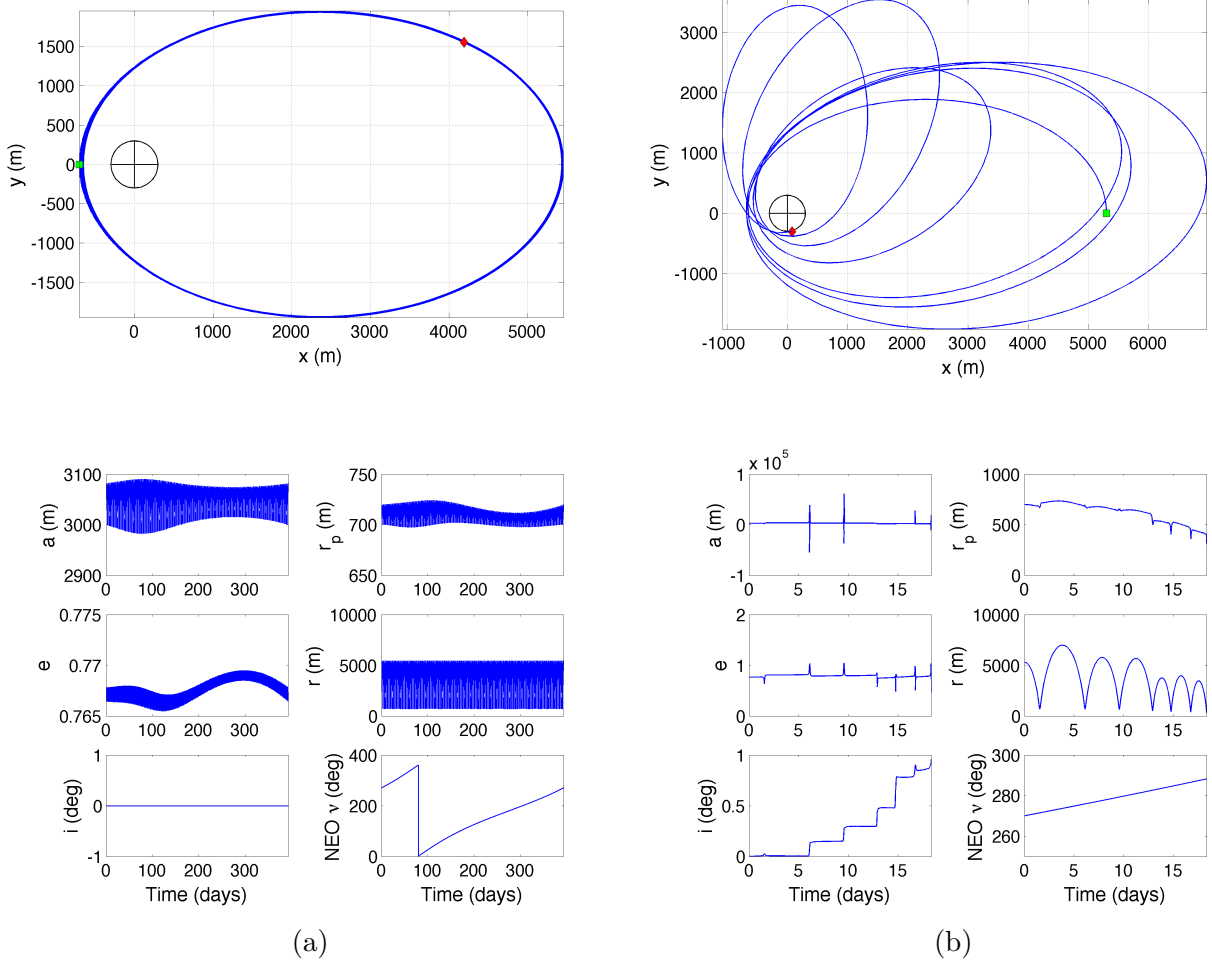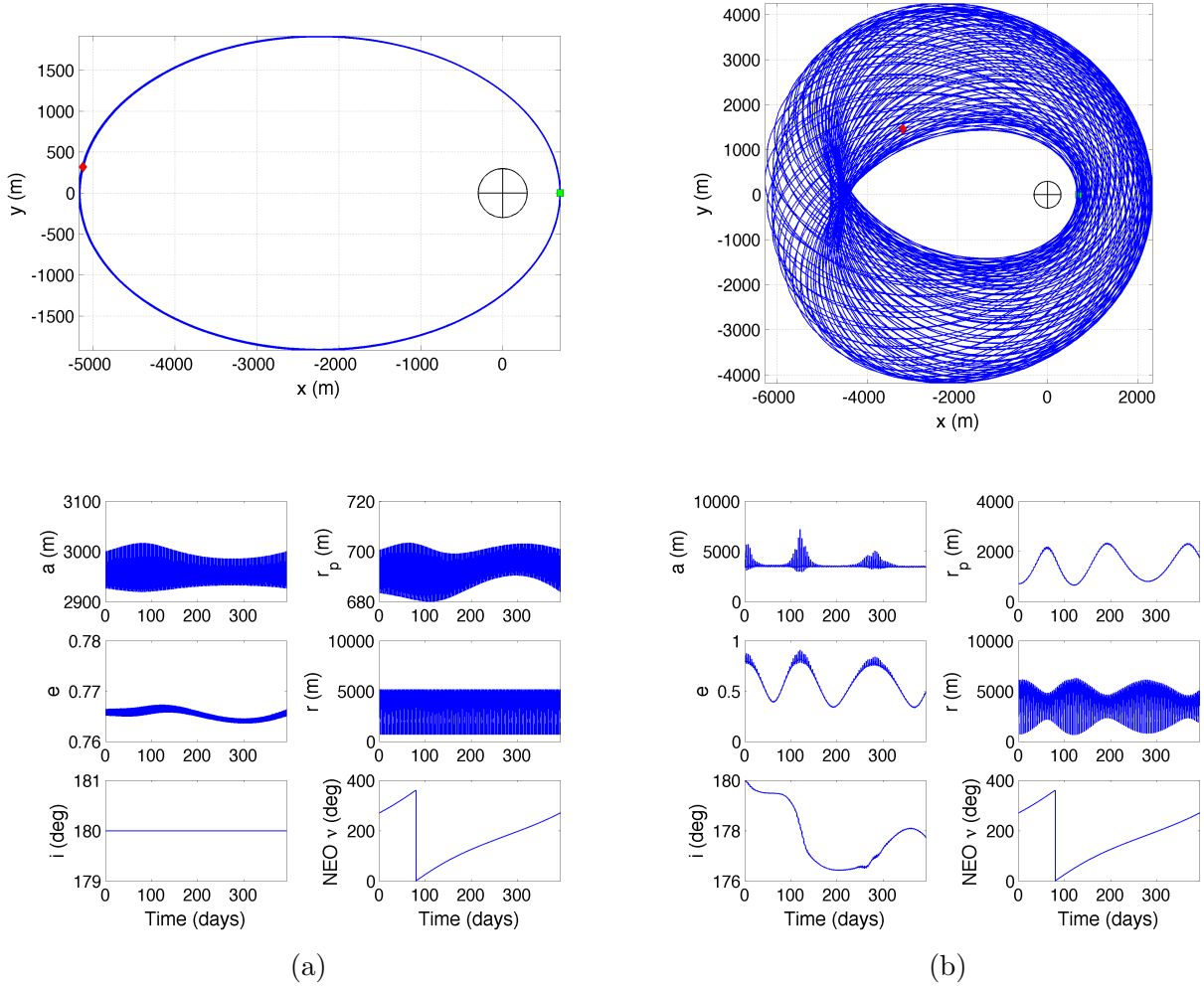
Figure 3.18: Retrograde ecliptic frozen orbit trajectory for an Orion-class spacecraft orbiting a medium-sized NEO ($[s, q, p] = [476.22032, 238.11016, 238.11016]$ m): (a) motion modeled with only the solar radiation pressure perturbation active; (b) motion modeled with all perturbations active. Like the prograde orbit in Figure 3.17, the retrograde orbit is also perturbed by the non-spherical distribution during each periapsis passage. However, unlike the prograde orbit, the retrograde orbit does not impact the NEO surface; in fact, it remains bound to the NEO throughout the propagation interval.

# Chapter 4

# Conclusions

A numerical model – including the perturbative effects of solar radiation pressure, solar gravity and a non-spherical mass distribution for the central body – was constructed to simulate orbital trajectories in close proximity to a small solar system body. Using this model, analytically-derived limits on the size of a stable orbit about a small body were confirmed numerically. For the particular application of a manned mission to a NEO, it was found that an Orion-class spacecraft can generally achieve a stable orbit about a NEO despite the presence of perturbations to the two body dynamics. The range of distances over which the spacecraft can orbit the NEO depends on the size and shape of the NEO, as well as the period of its rotation. The maximum limit on the semi-major axis size in the presence of the solar radiation pressure perturbation is found to be quite rigid, and increases in value with the NEO size (and therefore the NEO mass). The minimum limit on the semi-major axis threshold for guarding against ellipticity effects is found to more flexible, depending on the strength of the perturbation as quantified by the $\chi$ parameter. As the rotation period increases or the NEO shape becomes increasingly round, the perturbation due to the NEO ellipticity becomes increasingly weak and orbit stability is maintained for longer periods for orbits having semi-major axes less than $a_{\min}$. If the NEO is small enough and the rotation period long enough, the value of $a_{\min}$ can exceed that of $a_{\max}$. If the ellipticity perturbation is strong enough, these NEOs cannot be orbited at any distance. Finally, terminator frozen orbits have been shown to be the best orbit option a manned mission to a NEO. Their stability in the presence of multiple perturbation sources makes them the ideal solution for achieving a safe trajectory about the NEO

from which science observations can be made of the NEO and astronaut EVAs can be launched to the surface.

Future work in this area of research should investigate how the identified orbit solutions for an Orion-class spacecraft in close proximity to a NEO are affected by changes to one or more of the model parameters fixed for the purposes of the studies in this thesis. In particular, the dependence of orbit stability on the obliquity angle of the rotation axis and the $q : p$ ratio needs to be explored. The numerical model could also be enhanced in a number of ways. A more complex solar radiation pressure model could be implemented which monitors the orientation of each surface of the spacecraft relative to the incoming solar flux. In order to capture significantly more detailed features in the NEO surface morphology, higher order and degree gravity terms could be added to the shape model, and for the special case of real asteroids with well known shapes, a polyhedral model could be utilized for the NEO mass distribution. And finally, the modification to the equations of motion suggested in Equation 2.30 could be implemented to allow for simulation of orbits about extremely small NEOs.

# Bibliography

[1] Space Suit Evolution: From Custom Tailored to Off-The-Rack. `http://history.nasa.gov/spacesuits.pdf`.

[2] The Orion Service Module. `http://microgravity.grc.nasa.gov/Orion/ServiceModule/index.php`.

[3] Near-Earth Object Survey and Deflection Analysis of Alternatives. Report to Congress, NASA, March 2007.

[4] Seeking a Human Spaceflight Program Worth of a Great Nation. Technical report, Review of U.S. Human Spaceflight Plans Committee, 2009.

[5] P. A. Abell, D. Korsmeyer, R. Landis, T. Jones, D. Morrison, D. Adamo, L. Lemke, A. Gonzales, B. Gershman, T. Sweetser, L. Johnson, and E. Lu. Piloted Missions to Near-Earth Objects via the Crew Exploration Vehicle. In Bulletin of the American Astronomical Society, volume 38 of Bulletin of the American Astronomical Society, pages 422–+, October 2007.

[6] Japan Aerospace Exploration Agency. Identification of origin of particles brought back by Hayabusa. Press Release, November 2010. `http://www.jaxa.jp/press/2010/11/20101116_hayabusa_e.html`.

[7] R. R. Bate, D. D. Mueller, and J. E. White. Fundamentals of Astrodynamics. Dover Publications, Inc., 1971.

[8] R. H. Battin. Astronautical Guidance. McGraw-Hill Book Company, 1964.

[9] S. B. Broschart and D. J. Scheeres. Control of hovering spacecraft near small bodies: Application to asteroid 25143 itokawa. Journal of Guidance, Control, and Dynamics, 28(2):343–354, March-April 2005.

[10] B. Chauvineau and F. Mignard. Dynamics of binary asteroids. I - Hill's case. Icarus, 83:360–381, February 1990.

[11] N. A. Chuikova. The Gravitational Field and Figure of the Moon. Soviet Astronomy, 12:1021, June 1969.

[12] D. R. Davis, A. L. Friedlander, and T. D. Jones. Role of Near-Earth Asteroids in the Space Exploration Initiative., pages 619–655. Resources of near-earth space, 1993.

[13] D. P. Hamilton and J. A. Burns. Orbital stability zones about asteroids. Icarus, 92:118–131, July 1991.

[14] D. P. Hamilton and J. A. Burns. Orbital stability zones about asteroids. II - The destabilizing effects of eccentric orbits and of solar radiation. Icarus, 96:43–64, March 1992.

[15] S. Hatfield. Project Orion Overview and Prime Contractor Announcement. `http://www.nasa.gov/pdf/156298main_orion_handout.pdf`, August 2006.

[16] W. Hu and D. J. Scheeres. Numerical determination of stability regions for orbital motion in uniformly rotating second degree and order gravity fields. Planetary and Space Science, 52:685–692, July 2004.

[17] D. J. Korsmeyer, R. R. Landis, and P. A. Abell. Into the beyond: A crewed mission to a near-earth object. Acta Astronautica, 63:213–220, July-August 2008.

[18] MATLAB version 7.8.0.347 (R2009a). The MathWorks, Inc., Natick, Massachusetts, 2009.

[19] H. Schaub and J. L. Junkins. Analytical Mechanics of Space Systems. AIAA Education Series, 2003.

[20] D. J. Scheeres. Satellite Dynamics about Small Bodies: Averaged Solar Radiation Pressure Effects. Journal of Astronautical Sciences, 47(1):25–46, 1999.

[21] D. J. Scheeres. Orbit mechanics about small asteroids. 20th International Symposium on Space Flight Dynamics, September 2007.

[22] D. J. Scheeres, S. J. Ostro, R. S. Hudson, E. M. DeJong, and S. Suzuki. Dynamics of orbits close to asteroid 4179 toutatis. Icarus, 132:53–79, 1998.

[23] G. M. Szabó and L. L. Kiss. The shape distribution of asteroid families: Evidence for evolution driven by small impacts. Icarus, 196:135–143, July 2008.

[24] V. Szebehely. Theory of Orbits: The Restricted Problem of Three Bodies. Academic Press, 1967.

[25] S. J. Thornton and J. B. Marion. Classical Dynamics of Particles and Systems. Brooks/Cole Division of Thomson Learning, Inc., 5th edition, 2004.

[26] D. J. Vallado. Fundamentals of Astrodynamics and Applications. Space Technology Library, 3rd edition, 2007.